Published in final edited form as:
Neuroimage. 2021 January 15; 225: 117489. doi:10.1016/j.neuroimage.2020.117489.

Measurement reliability for individual differences in multilayer network dynamics: Cautions and considerations

Zhen Yang[a,b,*], **Qawi K. Telesford**[a], **Alexandre R. Franco**[a,b,c], **Ryan Lim**[a], **Shi Gu**[d], **Ting Xu**[c], **Lei Ai**[c], **Francisco X. Castellanos**[a,e], **Chao-Gan Yan**[f], **Stan Colcombe**[a,b], **Michael P. Milham**[a,c,*]

[a]Center for Biomedical Imaging and Neuromodulation, The Nathan S. Kline Institute for Psychiatric Research, 140 Old Orangeburg Rd, Orangeburg, NY 10962, United States

[b]Department of Psychiatry, NYU Grossman School of Medicine, 550 1st Avenue, New York, NY 10016, United States

[c]Center for the Developing Brain, The Child Mind Institute, 101 East 56th Street, New York, NY 10022, United States

[d]University of Electronic Science and Technology of China, Chengdu, Sichuan, China

[e]Department of Child and Adolescent Psychiatry, NYU Grossman School of Medicine, New York, NY 10016, United States

[f]CAS Key Laboratory of Behavioral Science, Institute of Psychology, Beijing, China

Abstract

Multilayer network models have been proposed as an effective means of capturing the dynamic configuration of distributed neural circuits and quantitatively describing how communities vary over time. Beyond general insights into brain function, a growing number of studies have begun to employ these methods for the study of individua differences. However, test–retest reliabilities for multilayer network measures have yet to be fully quantified or optimized, potentially limiting their utility for individual difference studies. Here, we systematically evaluated the impact of multilayer community detection algorithms, selection of network parameters, scan duration, and task condition on test–retest reliabilities of multilayer network measures (i.e., flexibility, integration, and recruitment). A key finding was that the default method used for community detection by the popular generalized Louvain algorithm can generate erroneous results. Although available, an updated algorithm addressing this issue is yet to be broadly adopted in the neuroimaging literature. Beyond the algorithm, the present work identified parameter selection as a key determinant of test–retest reliability; however, optimization of these parameters and expected reliabilities appeared to be dataset-specific. Once parameters were optimized, consistent with findings from the static functional connectivity literature, scan duration was a much stronger determinant of

[*]Corresponding authors at: Center for Biomedical Imaging and Neuromodulation, Nathan S. Kline Institute for Psychiatric Research, 140 Old Orangeburg Rd, Orangeburg, NY 10962, United States., zhen.yang@nki.rfmh.org, Zhen.yang@nki.rfmh.org (Z. Yang), michael.milham@childmind.org (M.P. Milham).

Supplementary materials
Supplementary material associated with this article can be found, in the online version, at doi: 10.1016/j.neuroimage.2020.117489.

reliability than scan condition. When the parameters were optimized and scan duration was sufficient, both passive (i.e., resting state, Inscapes, and movie) and active (i.e., flanker) tasks were reliable, although reliability in the movie watching condition was significantly higher than in the other three tasks. The minimal data requirement for achieving reliable measures for the movie watching condition was 20 min, and 30 min for the other three tasks. Our results caution the field against the use of default parameters without optimization based on the specific datasets to be employed – a process likely to be limited for most due to the lack of test–retest samples to enable parameter optimization.

Keywords

Reliability; Multilayer networks; Flexibility; Module allegiance; Scan duration; Naturalist viewing

1. Introduction

Following early seminal contributions (Watts and Strogatz, 1998; Barabasi and Albert, 1999), network science has played a pivotal role in revealing the structure and interactions of complex systems, such as social and transportation networks. More recently, this methodological approach has been applied to neuroscience, helping to further characterize the architecture of the human brain and launch the field of network neuroscience (Bullmore and Sporns, 2009; Bassett and Sporns, 2017). Accordingly, various tools have been developed to understand the brain as a complex network, highlighting variations in brain organization across development (Gu et al., 2015), aging (Voss et al., 2013), and clinical populations (Bassett et al., 2018). In many studies, brain networks are constructed from anatomic or functional neuroimaging data as a single network or static representation (Rubinov and Sporns, 2010; Sporns, 2013). As the human brain is intrinsically organized into functionally specialized modules, a common approach for analyzing brain networks is to investigate community structure, which identifies areas in the brain that are densely connected internally (Sporns and Betzel, 2016). While this construction is useful, a growing literature suggests that the brain, particularly its functional interactions, varies over time, thus necessitating the need to characterize these dynamic changes (Lurie et al., 2020).

Multilayer network models have been proposed as an effective means of capturing the temporal dependence between distributed neural circuits and quantitatively describing how communities vary over time (Mucha et al., 2010; Kivela et al., 2014). Multilayer network models can be used to optimize the partitioning of nodes into modules by maximizing a multilayer modularity quality function that compares edge weights in an observed network to expected edge weights in a null network. In this approach, two parameters are essential: the intra-layer coupling parameter, which tunes the number of communities within a layer, and the inter-layer coupling parameter, which tunes the temporal dependence of communities detected across layers. Dynamic network measures derived from multilayer modularity include but are not limited to flexibility, recruitment, and integration. Flexibility quantifies how frequently a region changes its community membership over time (Bassett et al., 2011); recruitment can be defined as the probability that a region is assigned to a community that is the same as its initial pre-defined network (e.g., visual, sensorimotor, or limbic network); and integration can be defined as the probability that a region is assigned to a community that is different from its initial pre-defined network (Bassett et al., 2015).

Initial applications of this approach have provided key insights into the brain network dynamics that underlie learning (Bassett et al., 2011, 2015). Recently, there has been increased enthusiasm to utilize these methods in the neuroimaging field (Table 1). Specifically, these measures have been used to link network dynamics to inter-individual differences in a broad range of functional domains, including motor learning (Bassett et al., 2011, 2015; Wymbs et al., 2012; Telesford et al., 2016), working memory (Braun et al., 2015; Finc et al., 2020), attention (Shine et al., 2016), language (Chai et al., 2016), mood (Betzel et al., 2017), creativity (Feng et al., 2019; He et al., 2019), and reinforcement learning (Gerraty et al., 2018). Additionally, dynamic network reconfiguration has been suggested as a potential biomarker for diseases, such as schizophrenia (Braun et al., 2016; Gifford et al., 2020), temporal lobe epilepsy (He et al., 2018), and depression (Wei et al., 2017; Zheng et al., 2018; Shao et al., 2019; Han et al., 2020), and has been used to predict antidepressant treatment outcome (Tian et al., 2020).

Despite these encouraging developments, several questions remain open. First, it is unclear whether there are optimal parameter values for characterizing community structure dynamics, and the extent to which parameter choice may affect the reliability of findings. Second, the minimum data requirements to obtain reliable estimates for multilayer network-based measures have not been established. Previous studies vary in scan duration from 5 min to 3.45 h (see Table 1). Third, how the choice of task during the scan (e.g., resting state, naturalistic viewing, or active tasks) impacts the reliability of multilayer network measurements has not been directly compared. As dynamic network methods become more widespread, a systematic evaluation of the impact of these important factors on the test–retest reliability of those derived measures is important and timely, given concerns about the reproducibility of neuroimaing research (Poldrack et al., 2017).

In this investigation, we aim to evaluate the impact of parameter selection, scan duration, and task condition on the test–retest reliabilities of dynamic measures obtained from multilayer modularity maximization (see Table 2 for an overview). We first identified the optimal intra-layer and inter-layer coupling parameters for the particular multilayer community detection algorithm that we employ, based on test–retest reliability. With the optimized parameters, we then evaluated test–retest reliability at various scan durations (i.e., 10, 20, 30, 40, 50, and 60 min) to determine the minimum data requirements for sufficient reliability. Given the growing popularity of naturalistic viewing, we examined reliability while participants were either watching Inscapes (Vanderwal et al., 2015) or movie clips (e.g., “The Matrix ”), as well as resting-state and a flanker task to directly quantify the modulatory effect of mental states. Importantly, given recent updates to dynamic community detection algorithms (Bazzi et al., 2016), we also evaluated the impact of algorithms on dynamic measurements and their test–retest reliability.

2. Material and methods

2.1. Datasets

Our primary analysis utilized data from the Healthy Brain Network-Serial Scanning Initiative (HBN-SSI: http://fcon_1000.projects.nitrc.org/indi/hbn_ssi/), a project specifically designed for evaluating the test–retest reliability of functional connectivity measures during different task states. Ten out of thirteen participants whose median framewise displacement (FD: Jenkinson et al., 2002) within 1.5 interqualtile range were included (29.8 ± 5.3 years, 50% males, median FD ranging from 0.04 to 0.08 mm). A detailed description of the experimental design and data collection can be found in O'Connor et al. (2017). Specific details on the flanker task can also be found in our Supplementary Materials. Briefly, each participant had 12 scanning sessions collected using the same imaging protocol over a 1–2-month period. At each session, a high-resolution structural image and four fMRI scans (i.e., resting state, Inscapes, movie, and flanker; 10 min/condition) were collected. All imaging data were collected using a 1.5 T Siemens Avanto MRI scanner equipped with a 32-channel head coil in a mobile trailer (Medical Coaches, Oneonta, NY). Structural scans were collected for registration using a multi-echo MPRAGE sequence (TR = 2.73 s, echo time = 1.64 ms, field of view = 256 × 256 mm^2, voxel size = 1.0 × 1.0 mm^3, flip angle = 7°). fMRI scans were collected using a multiband echo-planar imaging (EPI) sequence (multiband factor = 3, TR = 1.45 s, echo time = 40 ms, field of view = 192 × 192 mm^2, voxel size = 2.46 × 2.46 × 2.5 mm^3, flip angle = 55°).

To test the impact of implementation choices in the multilayer community detection code, we included resting-state fMRI data from 25 adults from the Human Connectome Project retest dataset (https://www.humanconnectome.org/study/hcp-young-adult/data-releases) (Van Essen et al., 2013), as well as created a simulated multilayer network dataset (see Supplementary Methods for details on these datasets). Furthermore, the generalizability of parameters optimized on the HBN-SSI dataset was evaluated on the HCP retest dataset.

2.2. Imaging preprocessing

Functional images were preprocessed using the Configurable Pipeline for the Analysis of Connectomes (C-PAC 1.3: http://fcp-indi.github.io/) with the following steps: (1) realignment to the mean EPI image to correct for motion; (2) nuisance signal regression: regressed out linear and quadratic trends, signals of the five principal components derived from white matter and cerebrospinal fluid (CompCor, Behzadi et al., 2007), global signal (Yang et al., 2014), and Friston 24-parameter motion model (Friston et al., 1996); and (3) spatial normalization of functional data to Montreal Neurological Institute (MNI) space by combining boundary based registration (BBR) (Greve and Fischl, 2009) and Advanced Normalization Tools (Avants et al., 2011). Because we are interested in the impact of both the event-related signals and the state evoked by the flanker task, we did not regress out task effects. See Fig. 1 for the flowchart summarizing the major steps of the current analytical framework.

2.3. Network construction

We defined nodes in the network using the functional parcellation from the CC200 atlas (Craddock et al., 2012) generated by a spatially constrained spectral clustering method. This functional parcellation consists of 200 ROIs covering the whole brain, each of which is homogeneous in its estimated functional connectivity. This commonly chosen atlas was previously used for studying static functional connectivity in the HBN-SSI dataset (O'Connor et al., 2017) and for evaluating the reproducibility and reliability of state-based temporal dynamic methods (Yang et al., 2014). To determine whether our results were sensitive to functional parcellations and the resolution of parcellations, we tested the robustness of our findings using the Schaefer 200 and 600 brain parcellations (Schaefer et al., 2018). After preprocessing, we extracted mean signals from each ROI and then applied a sliding window to the time series. The window length (~100 s, 68 TRs, no overlap) was selected based on a previous multilayer network study (Telesford et al., 2016), which demonstrated that the number of communities stabilizes at a window length of ~100 s and that the inter-region variance of flexibility peaks at a window size of 75–120 s across different cognitive tasks. Since we are interested in comparing the test–retest reliabilities of dynamic network measures among task conditions, we selected the window length of ~100 s to also capture low frequency fluctuations with a low cutoff at 0.01 Hz. However, we acknowledge that this window selection may not have sufficient temporal resolution to relate network dynamic changes to changing conditions in naturalistic viewing or in the flanker task.

For each window or layer, edges were estimated using wavelet coherence using the wavelet coherence toolbox (Grinsted et al., 2004) (http://grinsted.github.io/wavelet-coherence/). As the most commonly used edge estimation for multilayer network analyses (Table 1), wavelet coherence is robust to outliers (Achard et al., 2006) and has advantages in terms of its utility for estimating correlations between fMRI time series, which display slowly decaying positive autocorrelations or long memory (Zhang et al., 2016; Telesford et al., 2017). Specifically, magnitude-squared coherence C_{xy} between a given pair of regions (x, y) is a function of the frequency (f) and defined by the equation:

$$C_{xy}(f) = \frac{\left|F_{xy}(f)\right|^2}{F_{xx}(f)F_{yy}(f)},$$

where $F_{xy}(f)$ is the cross-spectral density between region x and region y. The variables $F_{xx}(f)$ and $F_{yy}(f)$ are the autospectral densities of signals from region x and region y, respectively. The mean of $C_{xy}(f)$ over the frequency band of interest, in our case 0.01–0.10 Hz, is defined as the edge weight between regions x and y. The range of wavelet coherence is bounded between 0 and 1. For each subject, we obtained a 200 × 200 × 6 (region × region × window) coherence matrix per task per session, which is coupled into a multilayer network by linking a node to itself in the preceding and the following windows or layers (Mucha et al., 2010; Bassett et al., 2011). Dynamic community detection was then performed for each session.

2.4. Dynamic community detection algorithm

Multiplex communities can be defined by modularity maximization (Mucha et al., 2010), spectral clustering (Lin et al., 2009; Michoel and Nachtergaele, 2012), or other data-mining approaches (Ströele et al., 2009, 2011, 2012). Among these methods, the optimization of multislice modularity is the most popular approach for fMRI research, possibly due to its feasibility of representing dynamic functional networks (Bassett et al., 2011, Bassett et al., 2013a, Bassett et al., 2013b). While there are numerous methods for determining community structure, here we used a Louvain-like locally greedy algorithm (Blondel et al., 2008). We chose this algorithm because: (1) it has been shown to outperform other community detection methods (Yang et al., 2016), (2) is most commonly used in the field of network neuroscience (Blondel et al., 2008), (3) has been adapted to multilayer network models (Mucha et al., 2010; Bassett et al., 2011, Bassett et al., 2013a), and (4) has been commonly used in studies linking multilayer network measures to cognition and disorders. For detecting communities, the multilayer modularity quality function (Q) is optimized (details given in Section 2.4.1) and is defined as in Mucha et al. (2010):

$$Q = \frac{1}{2\mu}\sum_{ijlr}\left\{\left(A_{ijl} - \gamma_l M_{ijl}\right)\delta_{lr} + \delta_{ij}\omega_{jlr}\right\}\left(\delta\left(g_{il}, g_{jr}\right)\right)$$

where μ is the sum of edge weights across all nodes and layers; δ_{ij} is the Kronecker's δ-function that equals 1 when $i = j$ and equals 0 otherwise. The element A_{ijl} gives the strength of the edge between nodes i and j in layer l, and the element M_{ijl} is the corresponding edge expected in a null model. Different choices of the null model in modularity could lead to different community structures (Sarzynska et al., 2016); based on the scope of the current paper, we adopted the widely used setting in the dynamic network reconfiguration papers: the Newman-Girvan null model which defines M_{ijl} as:

$$M_{ij1} = \frac{k_{il}k_{j1}}{2m_1},$$

where $m_1 = \frac{1}{2}\sum_{ij} A_{ij1}$ is the total edge weight in layer l. The variables k_{il} and k_{jl} are the intra-layer strengths of node i and node j in layer l, respectively. In the quality function, g_{il} represents the community assignment of node i in layer l, and g_{jr} represents the community assignment of node j in layer r. Finally, $\delta(g_{il}, g_{jr}) = 1$ if $g_{il} = g_{jr}$ and $\delta(g_{il}, g_{jr}) = 0$ if $g_{il} \neq g_{jr}$.

We performed multilayer community detection using the generalized Louvain package implemented in MATLAB (Lucas et al., 2011–2019). This method treats intra-layer and inter-layer edges as unique and assigns communities to regions in all layers. This allows for the investigation of communities that are coherent over time and simultaneously across layers. Moreover, as the community labels are consistent across layers, this avoids the common problem of community matching.

2.4.1. Algorithm selection—Optimization of the quality function or modularity (Q) includes two phases: community detection and community merging (Fig. 2). In the first phase, each node starts as its own community. Starting from a randomly chosen initial node, modularity is calculated after merging this node with every other community, one by one. Then all merges that increase modularity are identified. The default algorithm (Maximum Modularity Method: MMM) and the revised algorithm (Modularity Probability Method: MPM) differ in how the merge is selected. The MMM selects the merge that produces the highest increase in modularity. In the MPM, a probability is attached to all merges that increase modularity (the higher the proportion of modularity increases, the higher the probability). Afterward, a merge is chosen randomly, weighted by the probability distribution of modularity increases. If no improvement in modularity is found, the node is left unmerged. This process is then repeated sequentially for all other nodes. In the second phase, any multi-node community is merged and treated as a single node. Then the two phases are repeated until all communities are merged into a single community or no further improvement is possible.

The MMM was the default method implemented in the original code publicly released in 2011. The MPM was added in 2016 (Version 2.1) to address an abrupt change in the behavior of the default method when the inter-layer coupling parameter increased (see Bazzi et al., 2016 for details). This abrupt change was initially observed in financial data and has not been evaluated in neuroimaging data. Given that the default method was widely used in the fMRI literature, we evaluated the impact of the default and the improved methods on the values of dynamic network measures, as well as the reliability and validity of these measures before making a selection.

2.4.2. Parameter optimization—When optimizing multilayer modularity, we must choose values for the two parameters γ and ω. The parameter γ_l is the intra-layer coupling parameter for layer l, which defines how much weight we assign to the null network and controls the size of the communities detected within layer l. The parameter ω_{jlr} is the inter-layer coupling parameter, which defines the weight of the inter-slice edges that link node *j* to itself between layer l and layer *r*; this parameter controls the number of communities formed across layers. Here, following previous work in the neuroimaging literature (Table 1), these two parameters have been set as constants ($\gamma_l = \gamma$ and $\omega_{jlr} = \omega$) across layers. The choice of these two parameters is critical for multilayer modularity optimization, as they have a large impact on the detected community structure, as well as on the dynamic measures derived from multilayer communities (Bassett et al., 2013a; Mattar et al., 2015; Chai et al., 2016). Multilayer modularity approaches were also shown to detect spurious group differences in dynamic network measures when these parameters were set inappropriately (Lehmann et al., 2017). Here, we optimized these two parameters based on test–retest reliability. Specifically, we computed intra-class correlation coefficients (ICC) for each of the three dynamic network measures across a range of γ and ω for each of the four tasks. Specifically, we considered the space spanned by the following ranges: γ= [0.95, 1.3] and ω = [0.1, 3.0]. We determined these ranges by applying the criterion that the number of modules be ≥ 2 and ≤ 100. As the space for γ is much smaller than that for ω, a smaller increment of 0.05 was used for γ and an increment of 0.1 was used for ω. After estimating the ICC at each point in this space, we identified the parameter value pair that produced the largest ICC. The γ and ω pair that produced the largest ICC most frequently across the 12 conditions (3 dynamic network measures and 4 tasks) was chosen as the optimal one for the dataset.

In addition to ICC, we also used discriminability to quantify the reliability and optimize the parameters for multilayer network measurement. Discriminability is a non-parametric statistic to quantify the degree to which an individual's samples are relatively similar to one another, which can be used to measure reliability without restricting the data to be univariate and Gaussian distribution (Bridgford et al., 2019). Here, we computed the discriminability across the γ-ω plane for flexibility, integration, and recruitment separately. Considering n subjects, where each subject has s measurements, then we have $N = n \times s$ total measurements across subjects for a given dynamic measure. Then discriminability is computed in the following three steps: (1) Compute the distance (in this case the Euclidean distance) between all pairs of measurements, resulting in a $N \times N$ matrix; (2) For measurements of all subjects, compute the fraction of times that a within-subject distance is smaller than a between-subject distance, resulting in $N \times$ (s-1) numbers between 0 and 1. The discriminability of the dataset is the average of the above mentioned fractions, resulting in a single number between 0 and 1. A high discriminability indicates that within-subject measurements are more similar to one another than between-subject measurements, suggesting the measurement is more reliable. The calculation of discriminability is conducted using R package (https://github.com/ebridge2/Discriminability).

2.4.3. Other considerations—When implementing the GenLouvain method, we used fully weighted, unthresholded coherence matrices to minimize the known near degeneracy of the modularity landscape (Good et al., 2010). After applying this algorithm, the 200 ROIs were assigned to communities that spanned across layers. Due to the roughness of the modularity landscape (Good et al., 2010) and the stochastic nature of the algorithm (Blondel et al., 2008), the output of community detection often varies across optimizations. Thus, rather than focus on any single optimization, we computed the dynamic measures based on 100 optimizations, following the precedent of previous work (Bassett et al., 2011, Bassett et al., 2013a, Bassett et al., 2013b, 2015). Specifically, we first calculated network measures (see next section for details) for each run of the community detection algorithm, and then we averaged those measures over the 100 optimizations.

2.5. Calculation of dynamic network measures

For each participant, we computed the following measures to characterize the dynamics of the multilayer network based on the dynamic community structure detected in each optimization.

2.5.1. Flexibility—For each brain region, the flexibility is calculated as the number of times a brain region changes its community assignment across layers, divided by the number of possible changes, which is the number of layers minus 1 (Bassett et al., 2011). This measure characterizes a region's stability in community allegiance and can be used to differentiate brain regions into a highly stable core and a highly flexible periphery (Bassett et al., 2013b). Regions with high flexibility are thought to have a larger tendency to interact with different networks. Average flexibility across the brain is also computed to examine the global flexibility of the system.

2.5.2. Module allegiance—

The module allegiance matrix is the fraction of layers in which two nodes are assigned to the same community (Bassett et al., 2015). For each layer, a co-occurrence matrix (200 × 200) can be created based on the community assignment of each node pair. The element of the co-occurrence matrix is 1 if two nodes are assigned to the same community, and 0 otherwise. The module allegiance matrix is computed by averaging the co-occurrence matrices across layers, and the value of the matrix elements thus ranges from 0 to 1.

2.5.3. Integration and recruitment—

To quantify the dynamic functional interactions among sets of brain regions located within predefined functional systems (i.e., seven networks defined by Yeo et al., 2011), we computed two network measures based on the module allegiance matrix: recruitment and integration (Bassett et al., 2015). Recruitment can measure the fraction of layers in which a region is assigned to the same community as other regions from the same pre-defined system. The recruitment of region i in system S is defined as:

$$R_i^S = \frac{1}{n_S} \sum_{j \in S} P_{ij}$$

where n_S is the number of regions in S, and P_{ij} is the module allegiance between node i and node j. The integration of region i with respect to system S is defined as:

$$I_i^S = \frac{1}{N - n_S} \sum_{j \notin S} P_{ij}$$

where N is the total number of brain regions. Integration I_i^S measures the fraction of layers in which region i is assigned to the same community as regions from systems other than S.

2.6. Assessment of reliability

Test-retest reliability and between-code reliability were assessed with the ICC estimated using the following linear mixed model:

$$Y_{ij}(v) = \mu_{00}(v) + \theta_{i0}(v) + \varepsilon_{ij}(v),$$

where $Y_{ij}(v)$ represents the dynamic measure (i.e., flexibility, integration, or recruitment) for a given brain region v ($v = 1, 2\ldots, 200$), i indexes participants ($i = 1, 2, \ldots 10$), and j indexes either the session for analyses of test–retest reliability or the code implementation options for analyses of between-code reliability ($j = 1, 2$). Further, μ_{00} (v) is the intercept or a fixed effect of the group average dynamic measure at region v; θ_{i0} (v) is the random effect for the ith participant at region v; and $\varepsilon_{ij}(v)$ is the error term. The total variance of a given dynamic measure can be decomposed into two parts: (1) inter-individual variance across all participants $\left(\sigma_\theta^2 = \mathrm{Var}[\theta]\right)$, and (2) intra-individual variance for a single participant across two measurements $\left(\sigma_\varepsilon^2 = \mathrm{Var}[\varepsilon]\right)$. The reliability of each dynamic measure can then be calculated as:

$$\mathrm{ICC} = \frac{\sigma_\theta^2}{\sigma_\theta^2 + \sigma_\varepsilon^2}.$$

The model estimations were implemented using the linear mixed effect (lme) function from the nlme R package (http://cran.r-project.org/web/packages/nlme).

2.7. Determination of the minimal data requirement

To establish minimal data requirements for sufficient test–retest reliability, we compared ICC values of six scan durations: 10 min, 20 min, 30 min, 40 min, 50 min, and 60 min. Different scan durations were obtained by pseudo-randomly selecting 1, 2, 3, 4, 5, or 6 10-min sessions from 12 available sessions for each participant. Dynamic features were first computed for each of the 12 10-min sessions, and then averaged across the sessions that were selected for each scan duration. We did not compute the dynamic measures on concatenated time series data to avoid artifactually introducing community changes at the concatenation point. For each scan duration, ICC was estimated using linear mixed models. To increase the robustness of the results and to extract stable features, we repeated the analysis on 100 randomized samples for each duration. The same process was performed for each of the four tasks to determine the data necessary for each condition.

2.8. Determination of task dependency

To investigate how estimates of test–retest reliability might depend on task states, we first used hierarchical linear mixed models to assess between-condition and between-session reliability in the same model. Hierarchical linear mixed models separate the variations among task conditions (i.e., between-condition reliability) from variations between sessions (i.e., test–retest reliability) by estimating variance between participants, across the four task conditions (for the same participant), and between sessions within each condition (O’Connor et al., 2017). Our model took the following form:

$$Y_{\mathrm{ijk}}(\mathrm{v}) = \mu_{000}(\mathrm{v}) + \theta_{\mathrm{jk}}(\mathrm{v}) + \phi_{\mathrm{k}}(\mathrm{v}) + \varepsilon_{\mathrm{ijk}}(\mathrm{v}).$$

The dynamic measure for a given brain region v can be denoted as $\mathrm{Y}_{\mathrm{ijk}}(\mathrm{v})$, where *i* indexes over sessions, j indexes over conditions, and k indexes over participants. In this model, μ_{000} represents the intercept; θ_{jk} represents a random effect between sessions for the j-th condition of the k-th participant; ϕ_{k} represents a random effect for the *k*-th participant; and $\varepsilon_{\mathrm{ijk}}$ represents the error term. The variables θ_{jk}, ϕ_{k}, and $\varepsilon_{\mathrm{ijk}}$ are assumed to be independent and to follow a normal distribution with a zero mean. The total variances of a given dynamic measure can be decomposed into three parts: (1) variance between participants ($\sigma_\phi^2 = \mathrm{Var}[\phi]$); (2) variance between conditions for the same participant ($\sigma_\theta^2 = \mathrm{Var}[\theta]$); and (3) variance of the residual, indicating variance between sessions ($\sigma_\varepsilon^2 = \mathrm{Var}[\varepsilon]$). The reliability of each dynamic measure across conditions can be calculated as

$$\text{ICC (conditions)} = \frac{\sigma_{\phi}^{2}}{\sigma_{\phi}^{2} + \sigma_{\theta}^{2}},$$

and across sessions as

$$\text{ICC (sessions } \mid \text{ conditions)} = \frac{\sigma_{\phi}^{2} + \sigma_{\theta}^{2}}{\sigma_{\phi}^{2} + \sigma_{\theta}^{2} + \sigma_{\varepsilon}^{2}}.$$

Next, we estimated the test–retest reliability for each task using the simple linear mixed models described in Section 2.6. The main effect of task condition on ICC values was tested using a nonparametric Friedman test. The Wilcoxon signed-rank test was used for *post hoc* analyses to determine which tasks differed significantly in test–retest reliability. As ICCs consistently increase with scan duration (Laumann et al., 2015; Xu et al., 2016; O'Connor et al., 2017), hierarchical and simple linear mixed models were performed using 60 min of data (the optimal scan duration in the current sample) to determine the impact of task condition.

3. Results

3.1. Impact of modularity maximization algorithm

In 2016, a comprehensive examination of multilayer networks with financial data revealed an abrupt discontinuity in values across the γ-ω landscape when the Maximum Modularity Method (MMM; the default method) was used. These findings raised concerns about the robustness of MMM (see Fig. 5.4 in Bazzi et al., 2016). In our study, when we used MMM, we observed a similar discontinuity in multilayer network-based dynamic measures in two independent human brain imaging datasets (HBN-SSI and HCP), as well as in a simulated multilayer-network dataset (Fig. 3). When the updated Modularity Probability Method (MPM) was used, we no longer observed such apparent discontinuities. To compare the dynamic measures computed using these two methods, we assessed the between-method reliability of flexibility for the two algorithms. Consistent with our intuition, we found that most of the ICC values above the discontinuity were near zero, suggesting that flexibility values obtained using different randomization methods can differ dramatically in that portion of the parameter space. In addition to flexibility, we also investigated the impact of these two methods on integration and recruitment. We found that flexibility was the most impacted, integration was impacted less, and recruitment was the least impacted (Fig. S1). Furthermore, we found that the updated method produced measures with greater test–retest reliability than the default method (Fig. S2), and better recovered known underlying dynamics in the simulated data - especially in the portions of parameter space above the apparent discontinuity (See Figs. S3 and S4 for details). Thus, the updated method (MPM) was used in the present work.

3.2. Parameter optimization based on test–retest reliability

Because our goal is to optimize multilayer network-derived measures to study individual differences, we chose our parameters based on test–retest reliability scores. The parameter γ

is the intra-layer coupling parameter, which defines how much weight we assign to the null network and controls the size of communities detected within a layer. The parameter ω is an inter-layer coupling parameter which defines the weight of the inter-slice edges that link a node to itself between two consecutive layers; it controls the number of communities formed across layers. We found that the selection of γ and ω had a large impact on the test–retest reliability of dynamic network measures (Fig. 4). Depending on parameter choice, test–retest reliability can range from poor to good. Overall, recruitment (mean ICC across the landscape: 0.54 ± 0.11) is more reliable than integration (0.37 ± 0.17), and integration is more reliable than flexibility (0.30 ± 0.15). For each measure, the pattern of ICC values across the 2-dimensional parameter space is highly similar across tasks. For each task, the portions of the parameter space with good ICCs are consistent across measures. Thus, we were able to identify an optimal range of parameters generalizable across tasks and measures. For flexibility and integration, good ICCs (≥ 0.6) occur within a range of γ= [1.0–1.1] and ω = [1.7–3.0]. For recruitment, the range is broader: γ= [1.05–1.25] and ω = [1.2–3.0].

For the current analysis, we chose the parameters γ= 1.05 and ω = 2.05, which produce maximal ICC values in 7 of the 12 γ-ω planes and still produce relatively good ICC values (ICC > 0.65) in the other 5 γ-ω planes. Tuning ω up to 2.05 yielded low estimates of flexibility. In a previous study, when the ω value was too high, flexibility values followed a heavy-tailed distribution with most values of flexibility equal to zero (i.e., close to a static network representation) (Telesford et al., 2016). In our investigation, the distribution of flexibility did not resemble this heavy-tailed distribution (Fig. S5A), thus mitigating the potential concern that the parameter was tuned too high.

Because the ICC is determined by both within- and between-subject variability, good ICC could be caused by increased between-subject variability, decreased within-subject variability, or a combination of both. To understand the driver of this variation in test–retest reliability, we examined the landscape of dynamic measures, as well as the between- and within-subject variance of these dynamic measures. To make the variance values comparable, we normalized the between- and within-subject variance by the total variance. We found that the mean and variance of these dynamic measures also depended on the values chosen for γ and ω (Fig. S6). The parameter values associated with good ICC overlapped with areas showing high between-subject variability and low within-subject variability, and largely overlapped with areas that had relatively low values of the dynamic measures (with a few exceptions for integration).

When the MPM was used, we found that reliability was poor for the previously recommended and commonly used values of γ= 1 and ω = 1. To better understand this poor reliability, we compared the recommended parameter choice with our reliability-optimized set. We found that although the spatial maps of flexibility were similar between two parameter choices (r = 0.70), the magnitude of flexibility was much larger for [γ= 1, ω = 1] compared to [γ= 1.05, ω = 2.5]: 0.66 ± 0.01 vs 0.16 ± 0.01, respectively (Fig. S5A). In the reviewed literature, when [γ= 1, ω = 1] was used, the range of flexibility is typically < 0.25 (Table 1). This discrepancy is likely because previous studies used the MMM (Bassett et al., 2011, Bassett et al., 2013a, Bassett et al., 2013b, 2015; Telesford et al., 2016; Finc et al., 2020). The poor ICC of [γ= 1, ω = 1] (mean: 0.19 ± 0.21) relative to [γ= 1.05, ω = 2.5] (mean: 0.79 ± 0.08) when the updated method was used was driven by the much lower between- and higher within-subject variance for [γ= 1, ω = 1] compared to [γ= 1.05, ω = 2.5] (except for the visual cortex).

To test whether functional parcellation and the resolution of a parcellation have an impact on dynamic reconfiguration, we repeated our analysis using Schaefer et al. (2018) 200 and 600 functional parcellations. We found that our results are relatively stable across different parcellations with the same number of ROIs, but parcellation resolution has an impact on parameter selection. Specifically, ICC values and dynamic network measures are similar between the Schaefer 200 and Craddock 200 atlases, and the optimized γ-ω are identical for the two atlases (γ= 1.05 and ω = 2.5) (Fig. S7). However, when the number of ROIs increases from 200 to 600, values of dynamic reconfiguration measures increase and a higher γ value is required to achieve good ICC values (Fig. S8). The optimized γ-ω for this higher resolution atlas is: γ= 1.15 and ω = 2.6. These results suggest that higher resolution atlases may augment values for node reconfiguration measures by increasing the number of communities at parameters around γ= 1.05 and ω = 2.5. However, these measures are not reliable. Higher values for the inter-layer coupling parameter are needed to generate dynamic communities that span multiple layers and higher values for the intra-layer coupling parameter are needed to reduce the number of communities to a level comparable to that of a low-resolution atlas.

To test whether the optimized parameters are generalizable, we applied the same multilayer analysis to HCP data and evaluated the test–retest reliability of flexibility. Compared to results for the HBN-SSI data, areas with relatively better reliability were located at values with lower γ and higher ω for the HCP data, although flexibility values were lower. Importantly, we were unable to identify any parameter value pairs with an ICC ≥ 0.6 for the HCP data, and the overall reliability is poorer for the HCP data compared to HBN-SSI data (HBN-SSI mean: 0.30 ± 0.15; HCP mean: 0.19 ± 0.05) (Fig. 5). This can be explained by lower between-subject variability and higher within-subject variability in the HCP data. To investigate the impact of preprocessing, we repeated our analysis on the HCP data using publicly released extensively preprocessed data. We found that both the flexibility values and reliability for the HCP data were similar between CPAC and HCP preprocessing, though the average reliability across the γ-ω landscape is higher for the HCP pipeline (CPAC mean: 0.19 ± 0.05; HCP mean: 0.27 ± 0.04). These results suggest that parameters optimized in one dataset (e.g., HBN-SSI, HCP) and/or preprocessing strategy (e.g., HCP pipeline employed ICA-FIX, while the C-PAC based pipeline used CompCor and global singal regression) may not be optimal for others (See Fig. 5 for visualization of γ-ω landscapes for HBN-SSI: CPAC, HCP: CPAC, and HCP: Enhanced).

Furthermore, we tested whether parameters optimized based on ICC are generalizable to parameters optimized for discriminability - a reliability index that is applicable to multivariate data (e.g., full brain or connectome). Similar to ICC, we found that discriminability was highest for recruitment, followed by integration, and lowest for flexibility (Fig. S9). For recruitment, most discriminability values across the γ-ω plane were high (>0.9; Bridgford et al., 2019). For integration, high discriminability values were located in the portion of γ-ω with medium ICC. For flexibility, high discriminability values were located in the portion of γ-ω with small ICC. Our results illustrate that parameters optimized based on one criterion may not always be optimal for another criterion.

3.3. Data requirements for characterizing inter-individual differences in network dynamics

To establish the minimal data requirements for these types of analyses, we calculated the ICC for each measure and each task at six different scan durations: 10 min, 20 min, 30 min, 40 min, 50 min, and 60 min. Consistent with previous static analyses (Laumann et al., 2015; Xu et al., 2016; O’Connor et al., 2017), we found that the test–retest reliability of dynamic measures improves with increased scan duration, and that this pattern is consistent across tasks and dynamic network measures (Fig. 6). From 10 to 60 min, the largest improvement is from 10 to 20 min. After 40 min, most regions achieved good ICCs and improvements were less notable for longer scan durations. For regional and system-level variations in improvement of reliability as a function of scan duration, see Fig. S10.

Regarding the question of how much data is needed for sufficient reliability, the answer depends on the criteria, the task, and the measure. Here, we define good test–retest reliability as over 50% of ROIs with ICC ≥ 0.5 (Xu et al., 2016). For the movie condition, good test–retest reliability was achieved for all three measures at 20 min (81.5% of ROIs had an ICC ≥ 0.5 on average across all three measures) (Fig. 7). For the flanker condition, good reliability was achieved at 20 min for integration (83.0% of ROIs ICC ≥ 0.5) and recruitment (57.0% of ROIs ICC ≥ 0.5). For the rest and Inscapes conditions, good reliability was achieved at 20 min only for integration (52.0% and 55.5% of ROIs ICC ≥ 0.5, respectively). With 30 min of data, all measures and all tasks had good test–retest reliability. Across scan duration and task condition, integration is more reliable than recruitment (Wilcoxon signed-rank test: $p < 0.001$) and recruitment is more reliable than flexibility ($p = 0.02$).

When data for one task is insufficient, a potential solution is to combine data across different tasks to increase scan duration, and thus improve reliability (O’Connor et al., 2017; Elliott et al., 2019a). To test whether this approach is relevant to the types of analyses performed here, we compared the ICCs obtained from 10 min of resting state data with the ICCs obtained from 10 min of Inscapes, movie, or flanker task condition, as well as those obtained from longer data created by adding either more resting state data or data from the other three tasks (Fig. 8). We found that at 10 min, ICCs are poor for all four tasks (over 75% of ROIs with ICC < 0.4), with resting state the poorest (96.5% of ROIs with ICC < 0.4). With increased scan duration, the reliability for the pure task condition increases, with the movie condition having the most ROIs showing good ICC at each scan duration. When comparing pure resting state data with mixed data of the same duration, generally the pure data had a greater number of ROIs with good to excellent ICC compared to the mixed data. When comparing 10 min of resting state data with longer mixed data, we found that combining data from different tasks improved reliability. The degree of improvement depended more on how much data was combined, and less on what task conditions were combined.

3.4. Task modulation on test–retest reliability of network dynamics: hierarchical linear mixed model

To separate variation among scan conditions from variations between sessions, we assessed between-condition reliability and between-session reliability simultaneously in a hierarchical linear mixed model. With the optimized γ-ω and the maximal amount of data available (60 min), we found that both between-session (two sessions, 60 min/session) and between-condition (four conditions) reliability were excellent (between-session median ± interquartile range: flexibility, 0.76 ± 0.05; integration, 0.80 ± 0.02; recruitment, 0.77 ± 0.08; between-condition: flexibility, 0.74 ± 0.10; integration, 0.76 ± 0.07; recruitment, 0.77 ± 0.16) (Fig. 9). Consistent with previous work (O'Connor et al., 2017), we found that between-condition reliability of the visual and somatomotor network tended to be the poorest for recruitment which quantifies within-network functional interactions. Because different task states vary systematically in the richness of visual stimuli (movie > Inscapes > flanker > rest) and motor demands (flanker > the other three conditions), it is reasonable that these primary networks re-configure themselves according to unique task demands.

3.5. Task modulation on test–retest reliability of network dynamics: linear mixed model

Following the high-level model, we investigated test–retest reliability for each task separately using simple linear mixed models. We found that all four tasks have good to excellent test–retest reliability for all three measures (Fig. 10). Median ± interquartile range of ICC for rest, Inscapes, movie, and flanker were: flexibility (0.73 ± 0.09, 0.75 ± 0.09, 0.81 ± 0.07, 0.73 ± 0.08), integration (0.78 ± 0.05, 0.76 ± 0.05, 0.84 ± 0.04, 0.79 ± 0.05), and recruitment (0.74 ± 0.13, 0.74 ± 0.16, 0.81 ± 0.09, 0.76 ± 0.11). When reliability was directly compared between tasks, there was a significant main effect of task for all three measures (Friedman test: $p < 0.001$). Using *post hoc* testing, we found that the movie condition displayed significantly better test–retest reliability in all dynamic network measures than the other three conditions (Wilcoxon signed-rank test: all p-values < 0.001, Bonferroni corrected for 18 tests: 3 measures × 6 possible pairing).

For the comparison of the remaining conditions, the results were measure dependent. For flexibility, test–retest reliability in the Inscapes condition was significantly higher than in the flanker condition ($p < 0.001$, corrected), and the other comparisons were not significant; for integration, reliability differed significantly (flanker > rest > Inscapes, $p < 0.001$, corrected); for recruitment, reliability in the flanker condition was also significantly higher than in the rest and Inscapes conditions ($p < 0.001$, corrected). Generally, the reliability of these dynamic measures did not simply increase as a function of task engagement. Higher ICC scores were typically associated with relatively higher between-subject variance and lower within-subject variance (Fig. 10).

After considering overall reliability (median ICC), we next visualized regional and network differences in reliability between tasks. Consistent with overall results, we found that the movie condition exhibited higher reliability than the other three conditions in most brain regions/networks (Fig. 11). The other three conditions are similar to each other with a few exceptions: flexibility of the somatomotor, visual, and default mode networks, and recruitment of the visual and somatomotor networks. The observation that task effects were most robust within the primary cortices is consistent with the hierarchical linear mixed model and with previous work (O'Connor et al., 2017). Furthermore, we found that the spatial topographies of ICC differ among dynamic measures. This is expected because different measures capture different features of the dynamic community structure. Overall, the spatial variation of ICC was small for integration at 60 min (i.e., all regions showed good to excellent reliability) across conditions. The spatial topography for flexibility and recruitment seems more complex. For example, the visual cortex was most reliable for recruitment during the movie condition but least reliable for flexibility. These results may suggest that the likelihood that a visual region will be assigned to the same community as other visual network regions (quantified by recruitment) is stable during the movie watching condition when visual stimuli were continuously presented. However, the number of times that a visual region switches its community membership (captured by flexibility) is not as reliable.

3.6. Addressing concerns regarding head motion

Head motion remains a major concern for dynamic functional connectivity estimation (Yang et al., 2014; Bassett et al., 2018; Satterthwaite et al., 2019). In the present work, we only included participants with minimal head motion (median FD range: 0.04~0.08 mm). During preprocessing, we regressed out 24 motion-related parameters (Friston et al., 1996); as well as controlled motion with more generalized approaches such as global signal regression at the individual level (Yan et al., 2013; Yang et al., 2014; Lydon-Staley et al., 2019a). To provide further insights into this concern, we examined the correlation between head motion (median FD) and the global mean of each dynamic measure and no significant correlations were found. Furthermore, we re-estimated test–retest reliability for flexibility on the movie condition using the optimized parameter while including median FD as a covariate at the group level in the linear mixed model. We found similarly good reliability with and without head motion included in the model (ICC = 0.67 and 0.74, respectively), suggesting that the impact of head motion on test–retest reliability was small.

4. Discussion

Optimizing the reliability of dynamic network methods is key to accurately characterizing trait-like individual differences in brain function. The present work examined the impact of the modularity maximization algorithm, network parameter selection, scan duration, and task condition on the test–retest reliability of dynamic network measures obtained using multilayer network models. We found that each of these factors impacted reliability to differing degrees. As suggested by prior work, optimal parameter selection was found to be an important determinant of reliability; interestingly, our findings revealed a more complex story than previously appreciated, as reliability across the multivariate parameter space was found to depend on an update in the multilayer community detection algorithm. Consistent with findings from the static functional connectivity literature, scan duration was found to be a much stronger determinant of reliability than scan condition. As discussed in greater detail in the following sections, our findings suggest that rather than selecting a single set of parameters or methods previously used in the literature, optimization of multilayer network models per dataset is essential.

Multilayer network models of neural systems offer the potential to illuminate time-varying aspects of brain function that could not otherwise be revealed from traditional static network approaches. The aim of the present work is to quantify and optimize test–retest reliability for multilayer network models, establish minimum data requirements, and identify which task condition(s) can provide a reliable context in which to investigate time-invariant network dynamics. Although we only evaluated the reliability of the GenLouvain algorithm, which is one of the most popular algorithms, the framework presented can be applied to other software and multilayer network modularity-maximizing algorithms. With increased interest in linking the time-resolved reconfiguration of functional brain networks to normal cognition and disorders, it is important for the field to establish standards to guide the application of dynamic connectivity approaches. The present work systematically evaluated the impact of parameter selection, scan duration, and task condition on the test–retest reliability of dynamic network measures, which addresses an important gap in the literature. Although the present work focused on fMRI data, our analytical methods and results are broadly applicable, as multilayer network modeling has been widely applied to other neuroimaging modalities (e.g., structural MRI, EEG, MEG) and non-neuroimaging data, such as social, economic, gene, and protein networks (Boccaletti et al., 2014).

4.1. A cautionary note on the selection of GenLouvain algorithms

When using the GenLouvain algorithm for modularity maximization, a critical step is to merge nodes into communities. The MMM is the default method used in the implementation of this algorithm, which merges nodes that produce the highest increase in modularity. In 2016, a newer approach was introduced, the MPM, which selects merges based on the probability distribution of modularity increases. A previous study of financial data reported that when the default method was used, two computational issues arise in the multilayer setting: an under-emphasis of persistence and an abrupt drop in the number of intra-layer merges in certain portions of the parameter space - both of which can lead to an abrupt change in the quantitative measure derived (Bazzi et al., 2016). Here, when the default method was used, we observed an abrupt dropoff in the optimization landscape in brain imaging data as well as in synthesized data (Fig. 3).

The abrupt discontinuity in the γ-ω landscape is not a coding error. Instead, it is a reflection of how the edges are defined (e.g., functional neuroimaging datasets generally use normalized correlation/coherence values between regions/voxels), the relationship between the multilayer inherited parameters, and the strengths of edges. The abrupt change occurs when the inter-layer coupling parameter ($\underline{\boldsymbol{\omega}}$) is greater than the average intra-layer edge strength. As the optimization of the modularity function has proven to be non-deterministic polynomial-time-hard (Newman, 2006), the default deterministic algorithm suffers from local minimum issues and results in fewer merges - especially when ω values are high. In contrast, the probabilistic approach, with a mechanism analogous to a simulated annealing algorithm, is better suited to approximate the global optimum of the quality function (Bazzi et al., 2016). Using the probabilistic approach leads to more variability across multiple simulations for a given dataset, thus mitigating the abrupt change seen in the optimization landscape.

The fact that abrupt discontinuities were observed consistently regardless of data type raises concerns regarding the accuracy of dynamic measures derived using the default option and with parameters selected above the point of apparent discontinuity in the 2-dimensional parameter space. Based on these results, as well as our demonstration that the MPM has higher test–retest reliability and better validity compared to the MMM, we strongly recommend that investigators use the updated method for multilayer network analysis, especially when applied to ordinal or temporal networks. Caution should be taken when attempting to judge findings obtained with the MPM based on older findings obtained with the MMM.

4.2. Parameter optimization for multilayer network analyses

To detect community structure, we employed the most commonly used algorithm to maximize the multilayer modularity quality function (Mucha et al., 2010). Communities that are detected using this algorithm are highly dependent on free parameters (i.e., γ and ω), thus we aimed to explore the space defined by these parameters and identify optimal parameter selection ranges in terms of test–retest reliability. As one parameter may affect the other parameter's optimal setting, it can prove useful to optimize γ-ω jointly. Although several heuristics exist for choosing the "best " value of γ and ω (Bassett et al., 2013a; Chai et al., 2016; Weir et al., 2017), optimizing the ICC has not previously been proposed, possibly because it requires the acquisition of a retest dataset. Our results suggest that a systematic evaluation of the parameters in terms of reliability has marked utility, as parameter choices directly impact reliability.

In the 2-dimensional parameter space of the γ-ω plane, we were able to find a range of parameters that produced dynamic network measures with good reliability. For flexibility and integration, better reliability was achieved with higher ω (i.e., when there is a stronger temporal coupling) and lower γ (i.e., when there are fewer communities). For recruitment, good reliability was achieved with high ω and a wide range of γ from low to high. Stronger temporal coupling in a multilayer network is typically associated with lower temporal variability in network partitions over time. The good test–retest reliability obtained at high ω and low γ for flexibility and integration, may suggest that the temporal variability reserved after tuning up ω is composed of more between-subject variability than within-subject variability when the number of communities is small. The relative insensitivity of recruitment to the number of communities may be explained by our choice of predefined systems in which ROIs tend to be grouped together over time. These results suggest that ICC-guided parameter selection can potentially maximize between-subject variability and minimize within-subject variability. This practice is consistent with the recent call for including assessment and optimization for reliability as a common practice in neuroimaging, as it helps to improve statistical power and decrease the amount of data required per subject (Zuo et al., 2019).

A critical cautionary note for the identification of an optimal parameter set comes from the dependence of reliability across the 2-dimensional parameter space on the specific modularity maximization algorithm. A parameter choice of [γ= 1, ω = 1] was recommended in the literature based on modularity and partition similarity, as well as the differences between measures estimated on a real network compared to an appropriate multilayer network null model (Bassett et al., 2013a). Following these initial publications (Bassett et al., 2011, Bassett et al., 2013a), most studies have used [γ= 1, ω = 1] as their parameter choices (see Table 1) and tested the robustness of this parameter selection with small variations. Given this parameter choice falls in the dropoff area when the default MMM was used (Figs. 3 and S1) and it also falls in the poor test–retest reliability area when the updated MPM was used (Fig. S5), the parameter choice of [γ=1, ω = 1] needs to be reconsidered.

4.3. Generalizability of the optimized parameters to HCP data

To determine whether the parameters optimized for one dataset can be generalized to a different dataset, we compared the reliability landscapes from the HBN-SSI to those obtained with the HCP Test-Retest dataset. Recognizing the differences in preprocessing, we compared two datasets with identical preprocessing using CPAC. To investigate the impact of preprocessing, we also repeated the HCP analysis using the publicly released preprocessed data using the Enhanced HCP pipeline. We found that the reliability between the HCP Test (60 min) and Retest (60 min) data was much lower than that observed in the HBN-SSI dataset across the 2-dimensional γ-ω parameter space and this pattern was consistent regardless of preprocessing pipelines. One potential explanation for this difference between two datasets is that HCP data were acquired using faster sampling than the HBN-SSI data (TR: 0.72 s vs. 1.45 s). While static studies have indicated that increasing temporal resolution can either improve (Birn et al., 2013; Liao et al., 2013; Zuo et al., 2013) or have no impact (Horien et al., 2018) on reliability, the opposite was observed for dynamic analyses (Choe et al., 2017). In addition to TR, these two datasets were collected in scanners with different magnet strength (1.5 T vs 3 T) and used different multiband factors (3 vs 8 for HBN-SSI and HCP, respectively). Furthermore, although the subjects in the HCP and HBN-SSI were similar in terms of participant age and sex (HBN-SSI: 29.8 ± 5.3 years old, 50% males; HCP: 30.3 ± 3.3 years old, 36% males), intervals between acquistion of test and retest datasets differed. For the HBN-SSI, the sessions were acquired within two months, while the HCP has a large variation in test–retest interval (range from 52 to 326 days: 133.4 ± 58.3 days). These factors may impact the reliability of network flexibility assessment.

Importantly, our results raise significant concerns about the potential dependencies of ‘optimal parameters’ for multilayer network analysis on the datasets employed, beyond the specific properties identified in our work (i.e., amount of data per subject, or per condition). Demonstrating that test–retest reliability can differ substantially between datasets is a significant concern, as it suggests that parameters optimized in one dataset may not be optimal for others. Compounding the challenge at hand, few data collection efforts include test–retest samples, and few contain the amounts of data per subject that our analyses suggest may be needed to achieve sufficient reliability. These varying factors raise concerns about the appropriateness of applying this approach to datasets that do not have a retest sample. It is also important for future studies to assess the generalizability of parameter optimization to datasets harmonized for key aspects of undesirable non-biological sources of variation, such as scanner manufacturer, acquisition protocol, and preprocessing steps. If such datasets are not available, applying statistical harmonization techniques, such as

ComBat (i.e., combining batches) (Johnson et al., 2007; Fortin et al., 2018; Yu et al., 2018), may decrease unwanted site effects and optimize multilayer network analysis.

4.4. Minimal data requirements for obtaining reliable dynamic estimates

Many factors impact the test–retest reliability of functional connectivity-based measures, among which scan duration is one of the most important (Zuo and Xing 2014; Zuo et al., 2019). Establishing minimal data requirements to obtain reliable estimates is an active research area for static connectivity analysis (Van Dijk et al. 2010; Anderson et al., 2011; Birn et al., 2013; Liao et al., 2013; Zuo et al., 2013; Laumann et al., 2015; Xu et al., 2016; Noble et al., 2017; Tomasi et al., 2017). However, to date, few efforts have been made to determine the scan duration needed to obtain reliable estimates of dynamic network measures. Here, we found that the test–retest reliability of dynamic network measures was poor for 10 min of data; it improved greatly when data increased to 20 min for movie fMRI and to 30 min for the other scan conditions. While increased scan duration has consistently been shown to improve reliability, studies vary in conclusions about the necessary data required to obtain reliable estimates. Studies have suggested that 5–10 min of data are sufficient to achieve respectable test–retest reliability (Van Dijk et al. 2010; Liao et al., 2013; Zuo et al., 2013; Tomasi et al., 2017); importantly, these studies have either focused on the default and frontoparietal networks, which have better reliabilities than other functional networks, or used more complex derived measures than simple edgewise indices. More recent work has convergently reported a substantial improvement in reliability to a level more useful for characterizing trait-like individual differences when data are increased from 5 to 10 min to 20–30 min (Laumann et al., 2015; Xu et al., 2016; Noble et al., 2017; O’Connor et al., 2017; Elliott et al., 2019a). Our results are consistent with these static functional connectivity studies.

As temporal dynamic analyses are susceptible to spurious variations (Hutchison et al., 2013; Leonardi and Van De Ville 2015; Lehmann et al., 2017), one would assume more data are required to obtain reliable measures for dynamic analyses compared to static analyses. Instead, our data recommendations for estimating flexibility, recruitment, and integration from multilayer community detection analyses are comparable to those for static functional connectivity analysis (20–30 min). This result may reflect our having optimized the analyses for test–retest reliability. As previous multilayer network-based studies vary widely in scan duration (ranging from 5 min to 3.45 h: Table 1), it is crucial to establish minimal data requirements for the study of trait-like individual differences.

4.5. Improvement of test–retest reliability by combining different conditions

It may not be practical to collect 20–30 min of data for a single condition, which motivates the question of whether different conditions can be combined to increase scan duration and improve test–retest reliability. Our hierarchical linear mixed model revealed good between-condition reliability, as well as good between-session reliability. These results are consistent with previous static connectivity analysis using the HBN-SSI dataset which demonstrated good between-condition reliability (O’Connor et al., 2017). Our findings are also consistent with previous work showing that task and resting-state data share a large proportion of variance (Cole et al., 2014; Geerligs et al., 2015) and that inter-task variance is much smaller relative to inter-subject variance in functional connectivity (Finn et al., 2015; Gratton et al., 2018). Recent work leveraging shared features across resting-state and task fMRI using a method called ‘general functional connectivity’ has demonstrated that static intrinsic connectivity estimated based on a combination of task and resting-state data offers better test–retest reliability than that estimated from the same amount of resting state data alone (Elliott et al., 2019a). Here, we found that depending on how much data and what task conditions were combined, mixed data have either comparable or lower reliability compared to the same amount of pure resting state data. When compared to 10 min of resting state data, longer duration created by combining task and resting-state data had better relaibility. Extending our understanding beyond prior studies of static connectivity, our results support the feasibility of combining data from different task conditions to improve reliability when the desired amount of a single condition is not available.

4.6. Movie fMRI identified as the most reliable condition

Another factor that impacts test–retest reliability of brain imaging-based measures is experimental paradigm due to the condition-dependent nature of brain activities (Zuo et al., 2019). Multilayer networks have been used to assess network reconfiguration during resting state (Mattar et al., 2015; Betzel et al., 2017; Wei et al., 2017; He et al., 2018; Khambhati et al., 2018; Pedersen et al., 2018; Zheng et al., 2018; Al-Sharoa et al., 2019; Feng et al., 2019; He et al., 2019; Li et al., 2019; Shao et al., 2019; Tian et al., 2019; Lydon-Staley et al., 2019a, 2019b), as well as during controlled cognitive tasks (Bassett et al., 2011, 2015; Braun et al., 2015; Chai et al., 2016; Telesford et al., 2016; Schlesinger et al., 2017a, 2017b; Gerraty et al., 2018; Cooper et al., 2019). The present work extended previous studies by including naturalistic viewing paradigms which offer increased ecological validity. Naturalistic paradigms allow researchers to study highly interactive dynamic cognitive processes (Bottenhorn et al., 2019) and probe complex multimodal integration (Sonkusare et al., 2019). They are emerging as powerful tools for exploring brain function and characerizing individual differences, with the potential for clinical applications (Eickhoff et al., 2020). Thus, establishing test–retest reliability of these paradigms is critical for enhancing our understanding of cognition as it occurs more naturally and advancing biomarker discovery for psychiatric disorders. A recent meta-analysis revealed that the flexible cognition during naturalistic viewing involves a common set of networks that allow separate processing of different streams of information, as well as integration of relevant information (Bottenhorn et al., 2019).

Compared to a passive resting state and an active flanker condition, we found that the movie condition had the best test–retest reliability. These results are consistent with previous static network studies which suggested better test–retest reliability for movie conditions than resting state (Wang et al., 2017). Naturalistic viewing was shown to have enhanced ability to identify brain-behavioral correlations compared to conventional tasks (Cantlon and Li 2013; Vanderwal et al., 2019) and was less impacted by head motion (Vanderwal et al., 2015), especially for pediatric samples. Some have suggested that the better reliability may be explained by the enhanced ability of movie watching to detect inter-individual differences in functional connectivity that are unique at the individual level compared to resting state (Vanderwal et al., 2017); alternatively, findings might be related to the increased level of engagement for movies compared to resting state. The poorer reliability of the flanker condition compared to movies could be ascribed to its having been designed to minimize between-subject variance to “isolate ” a single cognitive process (Elliott et al., 2019b). Regardless of explanation, the present results support the utility of movie fMRI as a reliable context in which to investigate time-invariant network dynamics.

4.7. Limitations and future work

To estimate functional connectivity, we used wavelet coherence based on its predominance across similar studies in the literature (see Table 1), as well as due to its advantages in terms of denoising, robustness to outliers, and appropriateness for fMRI time series (Zhang et al., 2016). While wavelet coherence offers several advantages, it is a frequency-specific measure and does not utilize phase information (Percival and Walden, 2000). As such, wavelet coherence is not useful when the phase of the signal is critical. Ongoing work is examining the reliability of other connectivity estimation methods, such as the Pearson’s correlation coefficient (Bassett et al., 2011; Mattar et al., 2015; Chai et al., 2016; Pedersen et al., 2018), which is informed by both phase and frequency information and can be computed more swiftly. Future work should investigate how edge density and threshold as well as edge weight sign (i.e., inclusion/exclusion of negative correlations) might impact the reliability of the dynamic network measures studied here.

We focused our analyses on low frequency fluctuations (0.01–0.1 Hz). The poorer reliability of the flanker condition compared to the movie condition could reflect the fact that we ignored the high frequency signals in the flanker task. To evaluate this possibility, we assessed flanker data reliability at a higher frequency range: 0.1–0.3 Hz. This range was selected to avoid the noisy upper bound (with TR = 1.45 s, the highest frequency we can examine is 0.34 Hz). We found that the reliability of dynamic measures obtained in the low frequency signals of the flanker task was much higher than in the higher frequency signals (Fig. S11). This suggests that the low frequency signals carry more non-random between-subject variation for this task, and that the relatively poor reliability of the flanker condition compared to the movie condition cannot be explained by frequency.

We determined the size of the parameter space by considering the number of communities (≥ 2 and ≤ 100), and we estimated the ICC at each point in the 2-dimensional γ-ω parameter space at a relatively coarse scale (γ: 0.9–1.3 with increments of 0.05; ω: 0.1–3.0 with increments of 0.1). We note that this resolution is comparable to most previous work (Bassett et al., 2011, Bassett et al., 2013b; Braun et al., 2015, 2016; Chai et al., 2016; He et al., 2018). Recent extensions of the multilayer network approach have demonstrated that sweeping across a range of intra-coupling parameters can offer insights into the multi-scale hierarchical organization of the brain (Ashourvan et al., 2019). Moreover, such studies have demonstrated that inter- and intra-subject variability in modular structure are scale specific (Betzel et al., 2019). Thus, sampling community structure from more points in the γ, ω parameter space may provide a better characterization of the brain’s dynamic network reconfiguration.

Indeed, some algorithms have been developed recently which allow a more refined and efficient search for parameters, for example, the Convex Hull of Admissible Modularity

Partitions (CHAMP) (Weir et al., 2017). Unlike the traditional way of selecting parameters in which the optimal partitions obtained at each (γ, ω) were treated independently, CHAMP uses the union of all computed partitions to identify the convex hull of a set of linear subspaces. It can greatly reduce the number of partitions that can be considered for future analyses by eliminating all partitions that were suboptimal across a given range of parameter space. Although the CHAMP software package is currently in its early versions (https://github.com/wweir827/CHAMP), future work implementing these methodological updates can potentially facilitate the parameter optimization process and map the ICC landscape in greater detail.

We found that our parameter selection was stable across functional parcellations with the same resolution. However, it was sensitive to the resolution of a parcellation (i.e., number of ROIs of a parcellation). Recent work further demonstrated that functional parcel definitions change with task (Salehi et al., 2020a) and individualized functional networks reconfigure with cognitive state (Salehi et al., 2020b). Thus, another limitation of the present work is that we used fixed nodes and did not consider flexible functional nodes. It is important for future work to evaluate the test–retest reliability of multilayer network measures computed using flexible functional nodes and taking into consideration the resolution of a parcellation. As the network measures we computed are summary measures of dynamic reconfiguration, another limitation is that they did not have the temporal resolution to relate to changing conditions in the movie or flanker task.

A further limitation is that we optimized parameters based on the global mean of dynamic network measures computed across the whole brain. It is possible that each network may have different optimal parameters and the parameters optimized at the global level may not be optimal at the network level. It is important for future work to test this possibility and extend the current maximization framework further. Additionally, we fixed the values of γ and ω to be uniform across all layers as done in prior work (Table 1). Another extension of the present investigation is to devise heuristics for determining the values of these parameters in a layer-specific way, allowing for finer control over the features of detected communities.

Optimization of multilayer network measures for reliability has the potential to enhance our ability to use these measures and study trait-like brain-behavior relationships more efficiently (Choe et al., 2017; Zuo et al., 2019). Establishing good reliability is a key component of reproducible research (Nichols et al., 2017; Poldrack et al., 2017). However, good test–retest reliability does not necessarily correspond to high sensitivity to detect brain-behavior relationships (Noble et al., 2017). Thus, it is important for future work to investigate the functional relevance of reliability-optimized dynamic network measures, as well as to consider optimizing the multilayer modularity framework based on other factors, such as predictive accuracy (Dadi et al., 2019). Prior work suggests that pipelines optimized on predictive accuracy give the best prediction for diverse targets (including neurodegenerative diseases, neuropsychiatric diseases, drug impact, and psychological traits) across multiple datasets (Dadi et al., 2019). Thus, adding this new dimension as optimization target may enhance the ability of multilayer network measures to become fundamental tools to delineate meaningful brain-behavior relationships.

5. Conclusions

The application of dynamic (i.e., time-varying) graph measures to fMRI data is a rapidly growing area and there is a clear need in the network neuroscience field for reliable measures that can be used to find trait-like individual differences in cognition and disorders. Our results provide evidence that dynamic measures from the well-known multilayer community detection technique (multilayer modularity maximization) can be reliable when the updated multilayer community detection method is used, the parameters are optimized for reliability, and scan duration is sufficient. However, we do not assert that our results are directly applicable to any other dataset. Instead, we highlight concerns about generalizability arising from our difficulties finding a robust optimization that would generalize across the datasets tested. Our results caution the field that continued optimization of multilayer network models is needed before any single set of parameters or methods can be accepted as standard practice. Future work is needed to continue optimizing this framework by evaluating the impact of imaging parameters (e.g., sampling rate, multiband factor), preprocessing steps (e.g., global signal regression), and multilayer network analyses-related methodological decisions (e.g., window size, edge definition, number of optimizations) on reliability, as well as to optimize predictive accuracy.

Supplementary Material

Refer to Web version on PubMed Central for supplementary material.

Acknowledgments

The work presented here was primarily supported by the NYS Office of Mental Health (AF, FXC, MPM, SC, ZY) and NIMH awards U01MH099059 (MPM), R24MH114806 (MPM), R01AG047596 (SC, MPM), 1U54MH091657, and R01MH111439 (MPM). Additional funding was provided by gifts to the Child Mind Institute (CMI) from Phyllis Green and Randolph Cowen. We would also like to thank the many individuals who have provided financial support to the CMI Healthy Brain Network to make the creation and sharing of this resource possible. SG was supported by the National Natural Science Foundation of China [NSFC-61876032]. CGY was supported by NSFC-81671774. Data were provided in part by the Human Connectome Project, WU-Minn Consortium (Principal Investigators: David Van Essen and Kamil Ugurbil; 1U54MH091657) funded by the 16 NIH Institutes and Centers that support the NIH Blueprint for Neuroscience Research; and by the McDonnell Center for Systems Neuroscience at Washington University.

References

Achard S, Salvador R, Whitcher B, Suckling J, Bullmore E, 2006 A resilient, low-frequency, small-world human brain functional network with highly connected association cortical hubs. J. Neurosci. 26 (1), 63–72. [PubMed: 16399673]

Al-Sharoa E, Al-Khassaweneh M, Aviyente S, 2019 Tensor based temporal and multilayer community detection for studying brain dynamics during resting state fMRI. IEEE Trans. Biomed. Eng. 66 (3), 695–709. [PubMed: 29993516]

Anderson JS, Ferguson MA, Lopez-Larson M, Yurgelun-Todd D, 2011 Reproducibility of single-subject functional connectivity measurements. Am. J. Neuroradiol. 32 (3), 548–555. [PubMed: 21273356]

Ashourvan A, Telesford QK, Verstynen T, Vettel JM, Bassett DS, 2019 Multi-scale detection of hierarchical community architecture in structural and functional brain networks. PLoS One 14 (5), e0215520. [PubMed: 31071099]

Avants BB, Tustison NJ, Song G, Cook PA, Klein A, Gee JC, 2011 A reproducible evaluation of ANTs similarity metric performance in brain image registration. Neuroimage 54 (3), 2033–2044. [PubMed: 20851191]

Barabasi AL, Albert R, 1999 Emergence of scaling in random networks. Science 286 (5439), 509–512. [PubMed: 10521342]

Bassett DS, Porter MA, Wymbs NF, Grafton ST, Carlson JM, Mucha PJ, 2013a Robust detection of dynamic community structure in networks. Chaos 23 (1), 013142. [PubMed: 23556979]

Bassett DS, Sporns O, 2017 Network neuroscience. Nat. Neurosci. 20 (3), 353–364. [PubMed: 28230844]

Bassett DS, Wymbs NF, Porter MA, Mucha PJ, Carlson JM, Grafton ST, 2011 Dynamic reconfiguration of human brain networks during learning. Proc. Natl. Acad. Sci. USA 108 (18), 7641–7646. [PubMed: 21502525]

Bassett DS, Wymbs NF, Rombach MP, Porter MA, Mucha PJ, Grafton ST, 2013b Task-based core-periphery organization of human brain dynamics. PLoS Comput. Biol. 9 (9), e1003171. [PubMed: 24086116]

Bassett DS, Xia CH, Satterthwaite TD, 2018 Understanding the emergence of neuropsychiatric disorders with network neuroscience. Biol. Psychiatry Cogn. Neurosci. Neuroimaging 3 (9), 742–753. [PubMed: 29729890]

Bassett DS, Yang M, Wymbs NF, Grafton ST, 2015 Learning-induced autonomy of sensorimotor systems. Nat. Neurosci. 18 (5), 744–751. [PubMed: 25849989]

Bazzi M, Porter MA, Williams S, McDonald M, Fenn DJ, Howison SD, 2016 Community detection in termporal multilayer networks, with an application to correlation networks. Multiscale Model. Simul. 14 (1), 1–41.

Behzadi Y, Restom K, Liau J, Liu TT, 2007 A component based noise correction method (CompCor) for BOLD and perfusion based fMRI. Neuroimage 37 (1), 90–101. [PubMed: 17560126]

Betzel RF, Bertolero MA, Gordon EM, Gratton C, Dosenbach NUF, Bassett DS, 2019 The community structure of functional brain networks exhibits scale-specific patterns of inter- and intra-subject variability. Neuroimage 202, 115990. [PubMed: 31291606]

Betzel RF, Satterthwaite TD, Gold JI, Bassett DS, 2017 Positive affect, surprise, and fatigue are correlates of network flexibility. Sci. Rep. 7 (1), 520. [PubMed: 28364117]

Birn RM, Molloy EK, Patriat R, Parker T, Meier TB, Kirk GR, Nair VA, Meyerand ME, Prabhakaran V, 2013 The effect of scan length on the reliability of resting-state fMRI connectivity estimates. Neuroimage 83, 550–558. [PubMed: 23747458]

Blondel VD, Guillaume JL, Hendrickx JM, de Kerchove C, Lambiotte R, Lefebvre E, 2008 Fast unfolding of communities in large networks. J. Stat. Mech. Theory Exp. 2008 (10), 10008–10012.

Boccaletti S, Bianconi G, Criado R, Del Genio CI, Gomez-Gardenes J, Romance M, Sendina-Nadal I, Wang Z, Zanin M, 2014 The structure and dynamics of multilayer networks. Phys. Rep. 544 (1), 1–122. [PubMed: 32834429]

Bottenhorn KL, Flannery JS, Boeving ER, Riedel MC, Eickhoff SB, Sutherland MT, Laird AR, 2019 Cooperating yet distinct brain networks engaged during naturalistic paradigms: a meta-analysis of functional MRI results. Netw. Neurosci. 3 (1), 27–48. [PubMed: 30793072]

Braun U, Schafer A, Bassett DS, Rausch F, Schweiger JI, Bilek E, Erk S, Romanczuk-Seiferth N, Grimm O, Geiger LS, Haddad L, Otto K, Mohnke S, Heinz A, Zink M, Walter H, Schwarz E, Meyer-Lindenberg A, Tost H, 2016 Dynamic brain network reconfiguration as a potential schizophrenia genetic risk mechanism modulated by NMDA receptor function. Proc. Natl. Acad. Sci. USA 113 (44), 12568–12573. [PubMed: 27791105]

Braun U, Schafer A, Walter H, Erk S, Romanczuk-Seiferth N, Haddad L, Schweiger JI, Grimm O, Heinz A, Tost H, Meyer-Lindenberg A, Bassett DS, 2015 Dynamic reconfiguration of frontal brain networks during executive cognition in humans. Proc. Natl. Acad. Sci. USA 112 (37), 11678–11683. [PubMed: 26324898]

Bridgford EW, Wang S, Yang Z, Wang Z, Xu T, Craddock RC, Kiar G, Gray-Roncal W, Priebe CE, Caffo B, Milham M, Zuo XN, C.f.R.a. Reproducibility and Vogelstein JT (2019), "Optimal Experimental Deisgn for Big Data: Applications in Brain Imaging." BioRxiv.

Bullmore E, Sporns O, 2009 Complex brain networks: graph theoretical analysis of structural and functional systems. Nat. Rev. Neurosci. 10 (3), 186–198. [PubMed: 19190637]

Cantlon JF, Li R, 2013 Neural activity during natural viewing of Sesame Street statistically predicts test scores in early childhood. PLoS Biol. 11 (1), e1001462. [PubMed: 23300385]

Chai LR, Mattar MG, Blank IA, Fedorenko E, Bassett DS, 2016 Functional network dynamics of the language system. Cereb. Cortex 26 (11), 4148–4159. [PubMed: 27550868]

Choe AS, Nebel MB, Barber AD, Cohen JR, Xu Y, Pekar JJ, Caffo B, Lindquist MA, 2017 Comparing test-retest reliability of dynamic functional connectivity methods. Neuroimage 158, 155–175. [PubMed: 28687517]

Cocuzza CV, Ito T, Schultz D, Bassett DS, Cole MW, 2020. Flexible coordinator and switcher hubs for adaptive task control. J. Neurosci. 40 (36), 6949–6968. [PubMed: 32732324]

Cole MW, Bassett DS, Power JD, Braver TS, Petersen SE, 2014 Intrinsic and task-evoked network architectures of the human brain. Neuron 83 (1), 238–251. [PubMed: 24991964]

Cooper N, Garcia JO, Tompson SH, O'Donnell MB, Falk EB, Vettel JM, 2019 Time-evolving dynamics in brain networks forecast responses to health messaging. Netw. Neurosci. 3 (1), 138–156. [PubMed: 30793078]

Craddock RC, James GA, Holtzheimer PE 3rd, Hu XP, Mayberg HS, 2012 A whole brain fMRI atlas generated via spatially constrained spectral clustering. Hum. Brain Mapp. 33 (8), 1914–1928. [PubMed: 21769991]

Dadi K, Rahim M, Abraham A, Chyzhyk D, Milham M, Thirion B, Varoquaux G, Alzheimer's Disease Neuroimaging I, 2019 Benchmarking functional connectome-based predictive models for resting-state fMRI. Neuroimage 192, 115–134. [PubMed: 30836146]

Eickhoff SB, Milham MP, Vanderwal T, 2020 Towards clinical applications of movie fMRI. NeuroImage 217, 116860. [PubMed: 32376301]

Elliott ML, Knodt AR, Cooke M, Kim MJ, Melzer TR, Keenan R, Ireland D, Ramrakha S, Poulton R, Caspi A, Moffitt TE, Hariri AR, 2019a General functional connectivity: shared features of resting-state and task fMRI drive reliable and heritable individual differences in functional brain networks. Neuroimage 189, 516–532. [PubMed: 30708106]

Elliott ML, Knodt AR, Ireland D, Morris ML, Poulton R, Ramrakha S, Sison ML, Moffitt TE, Caspi A and Hariri AR (2019b), "Poor Test-retest Reliability of Task-fMRI: New Empirical Evidence and a Meta-Analysis." BioRxiv.

Feng Q, He L, Yang W, Zhang Y, Wu X, Qiu J, 2019 Verbal creativity is correlated with the dynamic reconfiguration of brain networks in the resting state. Front. Psychol. 10, 894. [PubMed: 31068873]

Finc K, Bonna K, He X, Lydon-Staley DM, Kuhn S, Duch W, Bassett DS, 2020. Dynamic reconfiguration of functional brain networks during working memory training. Nat. Commun. 11 (1), 2435. [PubMed: 32415206]

Finn ES, Shen X, Scheinost D, Rosenberg MD, Huang J, Chun MM, Papademetris X, Constable RT, 2015 Functional connectome fingerprinting: identifying individuals using patterns of brain connectivity. Nat. Neurosci. 18 (11), 1664–1671. [PubMed: 26457551]

Fortin JP, Cullen N, Sheline YI, Taylor WD, Aselcioglu I, Cook PA, Adams P, Cooper C, Fava M, McGrath PJ, McInnis M, Phillips ML, Trivedi MH, Weissman MM, Shinohara RT, 2018 Harmonization of cortical thickness measurements across scanners and sites. Neuroimage 167, 104–120. [PubMed: 29155184]

Friston KJ, Williams S, Howard R, Frackowiak RS, Turner R, 1996 Movement-related effects in fMRI time-series. Magn. Reson. Med. 35 (3), 346–355. [PubMed: 8699946]

Geerligs L, Rubinov M, Cam C, Henson RN, 2015 State and trait components of functional connectivity: individual differences vary with mental state. J. Neurosci. 35 (41), 13949–13961. [PubMed: 26468196]

Gerraty RT, Davidow JY, Foerde K, Galvan A, Bassett DS, Shohamy D, 2018 Dynamic flexibility in striatal-cortical circuits supports reinforcement learning. J. Neurosci. 38 (10), 2442–2453. [PubMed: 29431652]

Gifford G, Crossley N, Kempton MJ, Morgan S, Dazzan P, Young J, McGuire P, 2020 Resting state fMRI based multilayer network configuration in patients with schizophrenia. Neuroimage Clin. 25, 102169. [PubMed: 32032819]

Good BH, de Montjoye YA, Clauset A, 2010 Performance of modularity maximization in practical contexts. Phys. Rev. E Stat. Nonlinear Soft Matter Phys 81 (4 Pt 2), 046106.

Gratton C, Laumann TO, Nielsen AN, Greene DJ, Gordon EM, Gilmore AW, Nelson SM, Coalson RS, Snyder AZ, Schlaggar BL, Dosenbach NUF, Petersen SE, 2018 Functional brain networks are dominated by stable group and individual factors, not cognitive or daily variation. Neuron 98 (2), 439–452 e435. [PubMed: 29673485]

Greve DN, Fischl B, 2009 Accurate and robust brain image alignment using boundary-based registration. Neuroimage 48 (1), 63–72. [PubMed: 19573611]

Grinsted A, Moore JC, Jevrejeva S, 2004 Application of the cross wavelet transform and wavelet coherence to geophysical time series. Nonlinear Process. Geophys. 11, 561–566.

Gu S, Satterthwaite TD, Medaglia JD, Yang M, Gur RE, Gur RC, Bassett DS, 2015 Emergence of system roles in normative neurodevelopment. Proc. Natl. Acad. Sci. USA 112 (44), 13681–13686. [PubMed: 26483477]

Han S, Cui Q, Wang X, Li L, Li D, He Z, Guo X, Fan YS, Guo J, Sheng W, Lu F, Chen H, 2020. Resting state functional network switching rate is differently altered in bipolar disorder and major depressive disorder. Hum. Brain Mapp. 41 (12), 3295–3304. [PubMed: 32400932]

He L, Zhuang K, Li Y, Sun J, Meng J, Zhu W, Mao Y, Chen Q, Chen X, Qiu J, 2019 Brain flexibility associated with need for cognition contributes to creative achievement. Psychophysiology 56 (12), e13464. [PubMed: 31453642]

He X, Bassett DS, Chaitanya G, Sperling MR, Kozlowski L, Tracy JI, 2018 Disrupted dynamic network reconfiguration of the language system in temporal lobe epilepsy. Brain 141 (5), 1375–1389. [PubMed: 29554279]

Horien C, Noble S, Finn ES, Shen X, Scheinost D, Constable RT, 2018 Considering factors affecting the connectome-based identification process: comment on Waller et al. Neuroimage 169, 172–175. [PubMed: 29253655]

Hutchison RM, Womelsdorf T, Allen EA, Bandettini PA, Calhoun VD, Corbetta M, Della Penna S, Duyn JH, Glover GH, Gonzalez-Castillo J, Handwerker DA, Keilholz S, Kiviniemi V, Leopold DA, de Pasquale F, Sporns O, Walter M, Chang C, 2013 Dynamic functional connectivity: promise, issues, and interpretations. Neuroimage 80, 360–378. [PubMed: 23707587]

Jenkinson M, Bannister P, Brady M, Smith S, 2002 Improved optimization for the robust and accurate linear registration and motion correction of brain images. Neuroimage 17 (2), 825–841. [PubMed: 12377157]

Johnson WE, Li C, Rabinovic A, 2007 Adjusting batch effects in microarray expression data using empirical Bayes methods. Biostatistics 8 (1), 118–127. [PubMed: 16632515]

Khambhati AN, Mattar MG, Wymbs NF, Grafton ST, Bassett DS, 2018 Beyond modularity: fine-scale mechanisms and rules for brain network reconfiguration. Neuroimage 166, 385–399. [PubMed: 29138087]

Kivela M, Arenas A, Barthelemy M, Gleeson JP, Moreno Y, Porter MA, 2014 Multilayer networks. J. Complex. Netw. 2 (3), 203–271.

Laumann TO, Gordon EM, Adeyemo B, Snyder AZ, Joo SJ, Chen MY, Gilmore AW, McDermott KB, Nelson SM, Dosenbach NU, Schlaggar BL, Mumford JA, Poldrack RA, Petersen SE, 2015 Functional system and areal organization of a highly sampled individual human brain. Neuron 87 (3), 657–670. [PubMed: 26212711]

Lehmann BCL, White SR, Henson RN, Cam C, Geerligs L, 2017 Assessing dynamic functional connectivity in heterogeneous samples. Neuroimage 157, 635–647. [PubMed: 28578129]

Leonardi N, Van De Ville D, 2015 On spurious and real fluctuations of dynamic functional connectivity during rest. Neuroimage 104, 430–436. [PubMed: 25234118]

Li Q, Wang X, Wang S, Xie Y, Li X, Xie Y, Li S, 2019 Dynamic reconfiguration of the functional brain network after musical training in young adults. Brain Struct. Funct. 224 (5), 1781–1795. [PubMed: 31006071]

Liao XH, Xia MR, Xu T, Dai ZJ, Cao XY, Niu HJ, Zuo XN, Zang YF, He Y, 2013 Functional brain hubs and their test-retest reliability: a multiband resting-state functional MRI study. Neuroimage 83, 969–982. [PubMed: 23899725]

Lin Y−R, Sun J, Castro P, Konuru R, Sundaram H, Kelliher A, 2009 MetaFac: community discovery via relational hypergraph factorization. In: Proceedings of the 15th ACM SIGKDD International Conference on Knowledge Discovery and Data Mining, KDD'09, pp. 527–536.

Lucas GS, Bazzi JM, Jutla IS and Mucha PJ (2011–2019), "A Generalized Louvain Method for Community Detection Implemented in MATLAB."

Lurie DJ, Kessler D, Bassett DS, Betzel RF, Breakspear M, Keilholz S, Kucyi A, Liegeois R, Lindquist MA, McIntosh AR, Poldrack RA, Shine JM, Thompson WH, Bielezyk NZ, Douw L, Kraft D, Miller RL, Muthuraman M, Pasquini L, Razi A, Vidaurre D, Xie H, Calhoun VD, 2020 Questions and controversies in the study of time-varying functional connectivity in resting fMRI. Netw. Neurosci 4 (1), 30–69. [PubMed: 32043043]

Lydon-Staley DM, Ciric R, Satterthwaite TD, Bassett DS, 2019a Evaluation of confound regression strategies for the mitigation of micromovement artifact in studies of dynamic resting-state functional connectivity and multilayer network modularity. Netw. Neurosci. 3 (2), 427–454. [PubMed: 30793090]

Lydon-Staley DM, Kuehner C, Zamoscik V, Huffziger S, Kirsch P, Bassett DS, 2019b Repetitive negative thinking in daily life and functional connectivity among default mode, fronto-parietal, and salience networks. Transl. Psychiatry 9 (1), 234. [PubMed: 31534117]

Mattar MG, Cole MW, Thompson-Schill SL, Bassett DS, 2015 A functional cartography of cognitive systems. PLoS Comput. Biol. 11 (12), e1004533. [PubMed: 26629847]

Michoel T, Nachtergaele B, 2012 Alignment and integration of complex networks by hypergraph-based spectral clustering. Phys. Rev. E Stat. Nonlinear Soft Matter Phys 86 (5 Pt 2), 056111.

Mucha PJ, Richardson T, Macon K, Porter MA, Onnela JP, 2010 Community structure in time-dependent, multiscale, and multiplex networks. Science 328 (5980), 876–878. [PubMed: 20466926]

Newman ME, 2006 Modularity and community structure in networks. Proc. Natl. Acad. Sci. USA 103 (23), 8577–8582. [PubMed: 16723398]

Nichols TE, Das S, Eickhoff SB, Evans AC, Glatard T, Hanke M, Kriegeskorte N, Milham MP, Poldrack RA, Poline JB, Proal E, Thirion B, Van Essen DC, White T, Yeo BT, 2017 Best practices in data analysis and sharing in neuroimaging using MRI. Nat. Neurosci. 20 (3), 299–303. [PubMed: 28230846]

Noble S, Spann MN, Tokoglu F, Shen X, Constable RT, Scheinost D, 2017 Influences on the test-retest reliability of functional connectivity MRI and its relationship with behavioral utility. Cereb. Cortex 27 (11), 5415–5429. [PubMed: 28968754]

O'Connor D, Potler NV, Kovacs M, Xu T, Ai L, Pellman J, Vanderwal T, Parra LC, Cohen S, Ghosh S, Escalera J, Grant-Villegas N, Osman Y, Bui A, Craddock RC, Milham MP, 2017 The healthy brain network serial scanning initiative: a resource for evaluating inter-individual differences and their reliabilities across scan conditions and sessions. Gigascience 6 (2), 1–14.

Pedersen M, Zalesky A, Omidvarnia A, Jackson GD, 2018 Multilayer network switching rate predicts brain performance. Proc. Natl. Acad. Sci. USA 115 (52), 13376–13381. [PubMed: 30545918]

Percival DB, Walden AT, 2000 Wavelet methods for time series analysis. Cambridge University Press.

Poldrack RA, Baker CI, Durnez J, Gorgolewski KJ, Matthews PM, Munafo MR, Nichols TE, Poline JB, Vul E, Yarkoni T, 2017 Scanning the horizon: towards transparent and reproducible neuroimaging research. Nat. Rev. Neurosci. 18 (2), 115–126. [PubMed: 28053326]

Rubinov M, Sporns O, 2010 Complex network measures of brain connectivity: uses and interpretations. Neuroimage 52 (3), 1059–1069. [PubMed: 19819337]

Salehi M, Greene AS, Karbasi A, Shen X, Scheinost D, Constable RT, 2020a There is no single functional atlas even for a single individual: functional parcel definitions change with task. Neuroimage 208, 116366. [PubMed: 31740342]

Salehi M, Karbasi A, Barron DS, Scheinost D, Constable RT, 2020b Individualized functional networks reconfigure with cognitive state. Neuroimage 206, 116233. [PubMed: 31574322]

Sarzynska M, Leicht EA, Chowell G, Porter MA, 2016 Null models for community detection in spatially embedded, temporal networks. J. Complex Netw. 4 (3), 363–406.

Satterthwaite TD, Ciric R, Roalf DR, Davatzikos C, Bassett DS, Wolf DH, 2019 Motion artifact in studies of functional connectivity: characteristics and mitigation strategies. Hum. Brain Mapp. 40 (7), 2033–2051. [PubMed: 29091315]

Schaefer A, Kong R, Gordon EM, Laumann TO, Zuo XN, Holmes AJ, Eickhoff SB, Yeo BTT, 2018 Local-global parcellation of the human cerebral cortex from intrinsic functional connectivity MRI. Cereb. Cortex 28 (9), 3095–3114. [PubMed: 28981612]

Schlesinger KJ, Turner BO, Grafton ST, Miller MB, Carlson JM, 2017a Improving resolution of dynamic communities in human brain networks through targeted node removal. PLoS One 12 (12), e0187715. [PubMed: 29261662]

Schlesinger KJ, Turner BO, Lopez BA, Miller MB, Carlson JM, 2017b Age-dependent changes in task-based modular organization of the human brain. Neuroimage 146, 741–762. [PubMed: 27596025]

Shanmugan S, Cao W, Satterthwaite TD, Sammel MD, Ashourvan A, Bassett DS, Ruparel K, Gur RC, Epperson NC, Loughead J, 2020 Impact of childhood adversity on network reconfiguration dynamics during working memory in hypogonadal women. Psychoneuroendocrinology 119, 104710. [PubMed: 32563173]

Shao J, Dai Z, Zhu R, Wang X, Tao S, Bi K, Tian S, Wang H, Sun Y, Yao Z, Lu Q, 2019 Early identification of bipolar from unipolar depression before manic episode: evidence from dynamic rfMRI. Bipolar Disord. 21 (8), 774–784. [PubMed: 31407477]

Shine JM, Koyejo O, Poldrack RA, 2016 Temporal metastates are associated with differential patterns of time-resolved connectivity, network topology, and attention. Proc. Natl. Acad. Sci. USA 113 (35), 9888–9891. [PubMed: 27528672]

Sonkusare S, Breakspear M, Guo C, 2019 Naturalistic stimuli in neuroscience: critically acclaimed. Trends Cogn. Sci. 23 (8), 699–714. [PubMed: 31257145]

Sporns O, 2013 Structure and function of complex brain networks. Dialogues Clin. Neurosci 15 (3), 247–262. [PubMed: 24174898]

Sporns O, Betzel RF, 2016 Modular brain networks. Annu. Rev. Psychol. 67, 613–640. [PubMed: 26393868]

Ströele V, Oliveira J, Zimbrão G, Souza JM, 2009 Mining and analyzing multi-relational social networks. In: Proceedings of International Conference on Computational Science and Engineering, CSE’09, 4, pp. 711–716.

Ströele V, Silva R, Ferreria de Souza M, de Mello CER, Souza JM, Zimbrão G, Oliveira J, 2011 Identifying workgroups in Brazilian scientific social networks. J. Univ. Comput. Sci. 17, 1951–1970.

Ströele V, Zimbrão G, Souza JM, 2012 Modeling, mining and analysis of multi-relational scientific social network. J. Univ. Comput. Sci. 18, 1048–1068.

Telesford QK, Ashourvan A, Wymbs NF, Grafton ST, Vettel JM, Bassett DS, 2017 Cohesive network reconfiguration accompanies extended training. Hum. Brain Mapp. 38 (9), 4744–4759. [PubMed: 28646563]

Telesford QK, Lynall ME, Vettel J, Miller MB, Grafton ST, Bassett DS, 2016 Detection of functional brain network reconfiguration during task-driven cognitive states. Neuroimage 142, 198–210. [PubMed: 27261162]

Tian S, Chattun MR, Zhang S, Bi K, Tang H, Yan R, Wang Q, Yao Z, Lu Q, 2019 Dynamic community structure in major depressive disorder: a resting-state MEG study. Prog. Neuropsychopharmacol. Biol. Psychiatry 92, 39–47. [PubMed: 30572002]

Tian S, Sun Y, Shao J, Zhang S, Mo Z, Liu X, Wang Q, Wang L, Zhao P, Chattun MR, Yao Z, Si T, Lu Q, 2020. Predicting escitalopram monotherapy response in depression: the role of anterior cingulate cortex. Hum. Brain Mapp. 41 (5), 1249–1260. [PubMed: 31758634]

Tomasi DG, Shokri-Kojori E, Volkow ND, 2017 Temporal Evolution of brain functional connectivity metrics: could 7 min of rest be enough? Cereb. Cortex 27 (8), 4153–4165. [PubMed: 27522070]

Van Dijk KR, Hedden T, Venkataraman A, Evans KC, Lazar SW, Buckner RL, 2010 Intrinsic functional connectivity as a tool for human connectomics: theory, properties, and optimization. J. Neurophysiol. 103 (1), 297–321. [PubMed: 19889849]

Van Essen DC, M. SS, Barch DM, Behrens TE, Yacoub E, Ugurbil K, Consortium W-MH, 2013 The WU-minn human connectome project: an overview. Neuroimage 80, 62–79. [PubMed: 23684880]

Vanderwal T, Eilbott J, Castellanos FX, 2019 Movies in the magnet: naturalistic paradigms in developmental functional neuroimaging. Dev. Cogn. Neurosci. 36, 100600. [PubMed: 30551970]

Vanderwal T, Eilbott J, Finn ES, Craddock RC, Turnbull A, Castellanos FX, 2017 Individual differences in functional connectivity during naturalistic viewing conditions. Neuroimage 157, 521–530. [PubMed: 28625875]

Vanderwal T, Kelly C, Eilbott J, Mayes LC, Castellanos FX, 2015 Inscapes: a movie paradigm to improve compliance in functional magnetic resonance imaging. Neuroimage 122, 222–232. [PubMed: 26241683]

Voss MW, Wong CN, Baniqued PL, Burdette JH, Erickson KI, Prakash RS, McAuley E, Laurienti PJ, Kramer AF, 2013 Aging brain from a network science perspective: something to be positive about? PLoS One 8 (11), e78345. [PubMed: 24223147]

Wang J, Ren Y, Hu X, Nguyen VT, Guo L, Han J, Guo CC, 2017 Test-retest reliability of functional connectivity networks during naturalistic fMRI paradigms. Hum. Brain Mapp. 38 (4), 2226–2241. [PubMed: 28094464]

Watts DJ, Strogatz SH, 1998 Collective dynamics of ‘small-world’ networks. Nature 393 (6684), 440–442. [PubMed: 9623998]

Wei M, Qin J, Yan R, Bi K, Liu C, Yao Z, Lu Q, 2017 Abnormal dynamic community structure of the salience network in depression. J. Magn. Reson. Imaging 45 (4), 1135–1143. [PubMed: 27533068]

Weir WH, Emmons S, Gibson R, Taylor D, Mucha PJ, 2017 Post-processing partitions to identify domains of modularity optimization. Algorithms 10 (3), 93–114. [PubMed: 29046743]

Wymbs NF, Bassett DS, Mucha PJ, Porter MA, Grafton ST, 2012 Differential recruitment of the sensorimotor putamen and frontoparietal cortex during motor chunking in humans. Neuron 74 (5), 936–946. [PubMed: 22681696]

Xia M, Wang J, He Y, 2013 BrainNet Viewer: a network visualization tool for human brain connectomics. PLoS One 8 (7), e68910. [PubMed: 23861951]

Xu T, Opitz A, Craddock RC, Wright MJ, Zuo XN, Milham MP, 2016 Assessing variations in areal organization for the intrinsic brain: from fingerprints to reliability. Cereb. Cortex 26 (11), 4192–4211. [PubMed: 27600846]

Yan CG, Cheung B, Kelly C, Colcombe S, Craddock RC, Di Martino A, Li Q, Zuo XN, Castellanos FX, Milham MP, 2013 A comprehensive assessment of regional variation in the impact of head micromovements on functional connectomics. Neuroimage 76, 183–201. [PubMed: 23499792]

Yang Z, Algesheimer R, Tessone CJ, 2016 A comparative analysis of community detection algorithms on artificial networks. Sci. Rep. 6, 30750. [PubMed: 27476470]

Yang Z, Craddock RC, Margulies DS, Yan CG, Milham MP, 2014 Common intrinsic connectivity states among posteromedial cortex subdivisions: insights from analysis of temporal dynamics. Neuroimage 93 (Pt 1), 124–137. [PubMed: 24560717]

Yeo BT, Krienen FM, Sepulcre J, Sabuncu MR, Lashkari D, Hollinshead M, Roffman JL, Smoller JW, Zollei L, Polimeni JR, Fischl B, Liu H, Buckner RL, 2011 The organization of the human cerebral cortex estimated by intrinsic functional connectivity. J. Neurophysiol. 106 (3), 1125–1165. [PubMed: 21653723]

Yu M, Linn KA, Cook PA, Phillips ML, McInnis M, Fava M, Trivedi MH, Weissman MM, Shinohara RT, Sheline YI, 2018 Statistical harmonization corrects site effects in functional connectivity measurements from multi-site fMRI data. Hum. Brain Mapp. 39 (11), 4213–4227. [PubMed: 29962049]

Zhang Z, Telesford QK, Giusti C, Lim KO, Bassett DS, 2016 Choosing wavelet methods, filters, and lengths for functional brain network construction. PLoS One 11 (6), e0157243. [PubMed: 27355202]

Zheng H, Li F, Bo Q, Li X, Yao L, Yao Z, Wang C, Wu X, 2018 The dynamic characteristics of the anterior cingulate cortex in resting-state fMRI of patients with depression. J. Affect. Disord. 227, 391–397. [PubMed: 29154155]

Zuo XN, Xing XX, 2014 Test-retest reliabilities of resting-state FMRI measurements in human brain functional connectomics: a systems neuroscience perspective. Neurosci. Biobehav. Rev. 45, 100–118. [PubMed: 24875392]

Zuo XN, Xu T, Jiang L, Yang Z, Cao XY, He Y, Zang YF, Castellanos FX, Milham MP, 2013 Toward reliable characterization of functional homogeneity in the human brain: preprocessing, scan duration, imaging resolution and computational space. Neuroimage 65, 374–386. [PubMed: 23085497]

Zuo XN, Xu T, Milham MP, 2019 Harnessing reliability for neuroscience research. Nat. Hum. Behav. 3 (8), 768–771. [PubMed: 31253883]

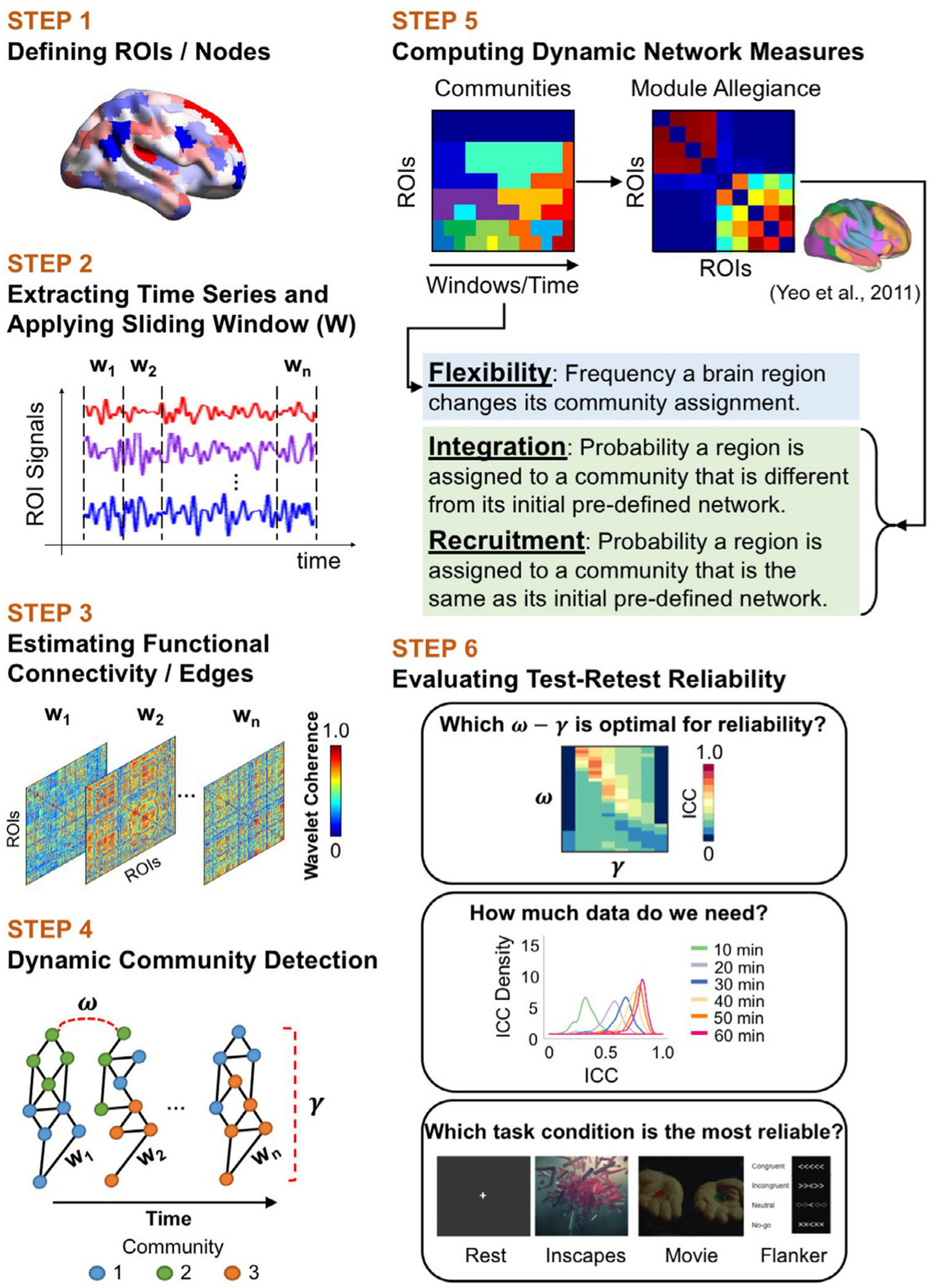

Flexibility: Frequency a brain region changes its community assignment.

Integration: Probability a region is assigned to a community that is different from its initial pre-defined network.

Recruitment: Probability a region is assigned to a community that is the same as its initial pre-defined network.

Fig. 1.

Flowchart summarizing the major steps of the current analytical framework.

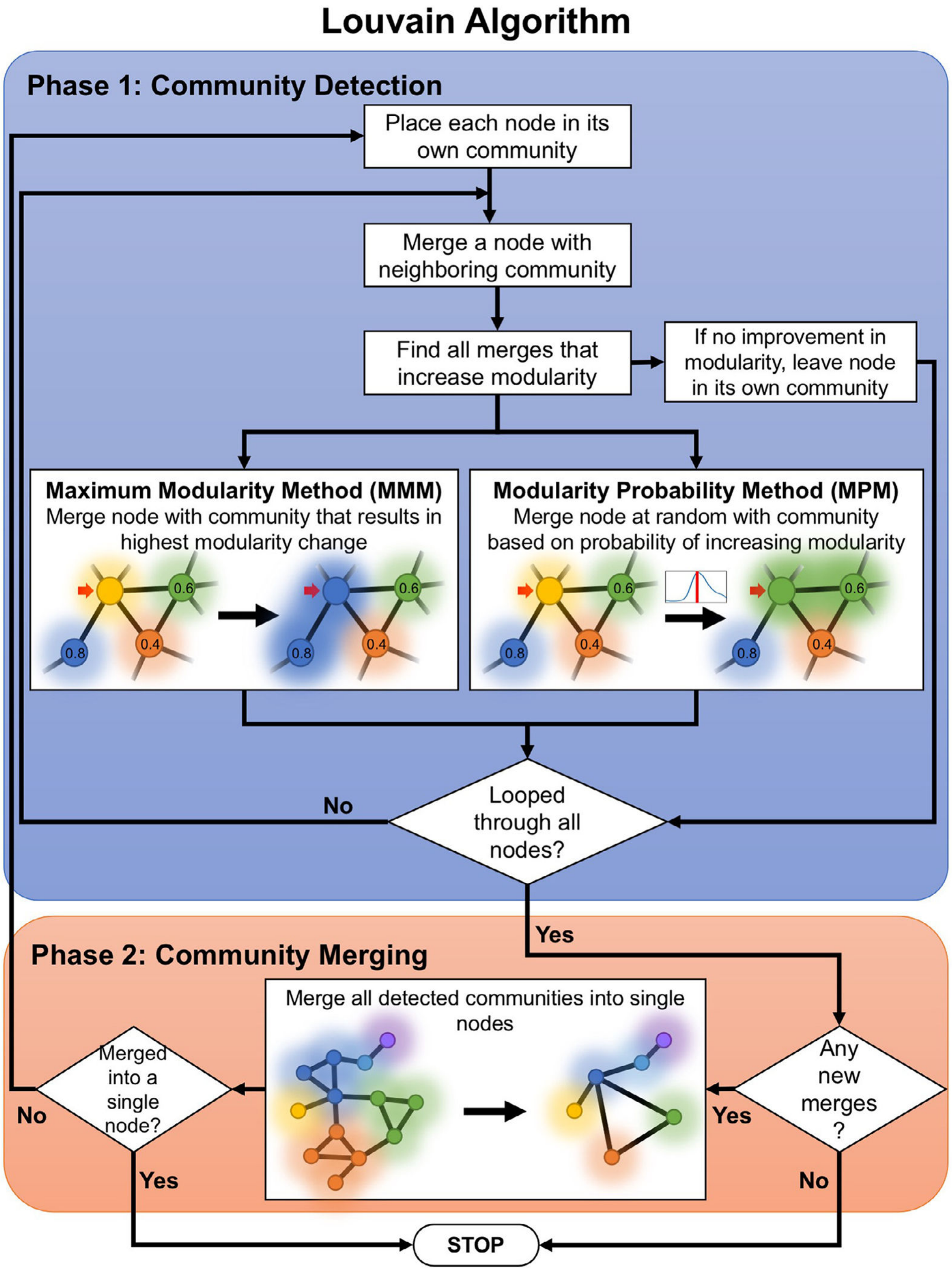
Louvain Algorithm
Phase 1: Community Detection
Place each node in its own community
Merge a node with neighboring community
Find all merges that increase modularity
If no improvement in modularity, leave node in its own community
Maximum Modularity Method (MMM)
Merge node with community that results in highest modularity change
0.6
0.8
0.4
0.6
0.8
0.4
Modularity Probability Method (MPM)
Merge node at random with community based on probability of increasing modularity
0.6
0.8
0.4
0.6
0.8
0.4
No
Looped through all nodes?
Yes
Phase 2: Community Merging
Merge all detected communities into single nodes
Merged into a single node?
No
Yes
Any new merges ?
Yes
No
STOP

Fig. 2.

Diagram showing the modularity maximization process. The generalized Louvain algorithm is a two-phase process that finds communities in a network. In the first phase, every node is placed in its own community. At random a node is merged with a neighboring community and modularity is calculated; after iterating through all available communities, a node can be merged with a community based on different methods. In the Maximum Modularity Method (MMM), the merge that resulted in the greatest increase in modularity is chosen. In the Modularity Probability Method (MPM), a community is chosen at random based on the probability that it increases the modularity. This process continues sequentially for all nodes until there are no improvements (no increase in modularity). In the second phase, detected communities are merged into single nodes and the process is repeated again. The algorithm ends if all nodes merge into a single community or if there are no improvements in modularity after iterating through nodes.

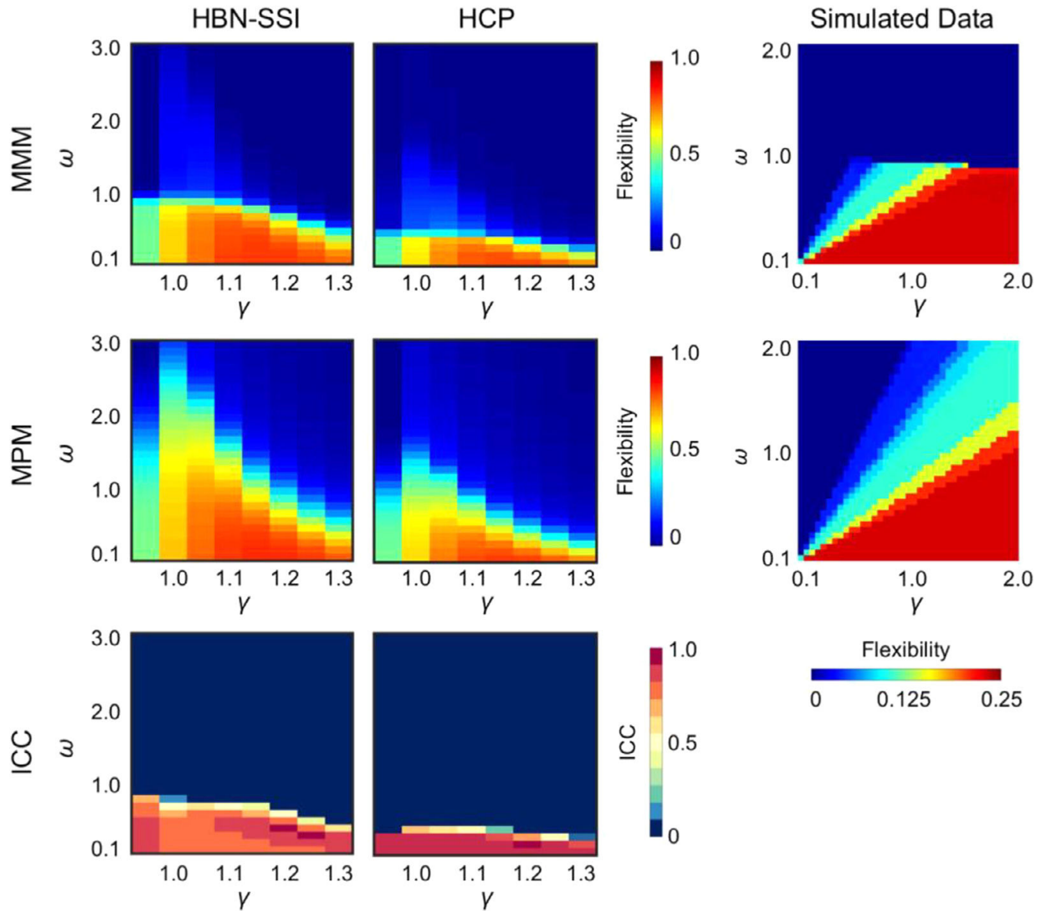

Fig. 3.

The impact of generalized Louvain method on estimated values of flexibility. When the default Maximum Modularity Method (MMM) was used, there was a dropoff in flexibility values in the 2-dimensional γ-ω parameter space (Top row). This apparent discontinuity was observed in two independent human brain imaging datasets, the Healthy Brain Network-Serial Scanning Initiative (HBN-SSI) and the Human Connectome Project (HCP), as well as in simulated data. The issue was mitigated by the updated Modularity Probability Method (MPM: Middle row). Reliability between flexibility values obtained using MMM and MPM was quantified using intra-class correlation coefficients (ICCs; Bottome row). ICCs were good below the apparent discontinuity and was near zero above the discontinuity. Brain Imaging results were obtained based on 60 min of resting state data.

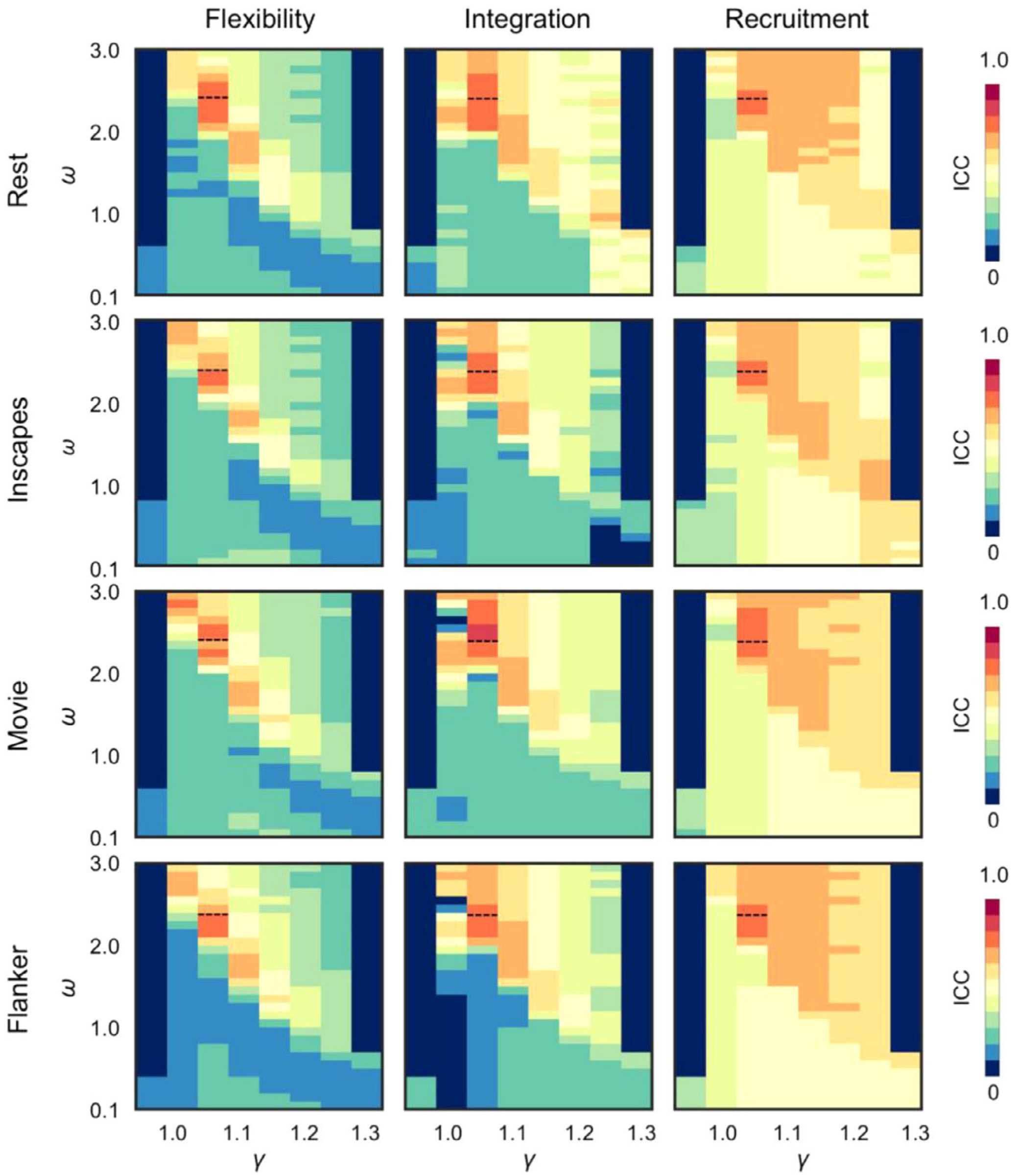

Fig. 4.

Test–retest reliability of dynamic network measures depends on the γ-ω selection. Based on global ICC computed across 200 ROIs (Craddock et al., 2012), we identified a range of parameters that produced good test-retest reliability (ICC ≥ 0.6) for three measures (flexibility, integration, and recruitment) and four tasks (rest, Inscapes, movie, and flanker). For a given measure, global ICCs were highly similar across tasks (compare rows). For a given task, the locations of good ICCs were consistent across measures (compare columns). The peak ICC value was observed in the same location (γ= 1.05, ω = 2.05) in 7 out of the 12 two-dimensional γ-ω planes (highlighted by a black dashed line). The ICC score at this location was also good (>0.65) in the other 5 two-dimensional γ-ω planes. Thus, this parameter value pair was chosen as the optimal γ-ω values for our analyses. Note that the values in the parameter space where the number of communities was smaller than 2 or greater than 100 were set to zero in each plane. ICCs were evaluated with the maximal amount of data available (60 min) in the HBN-SSI dataset.

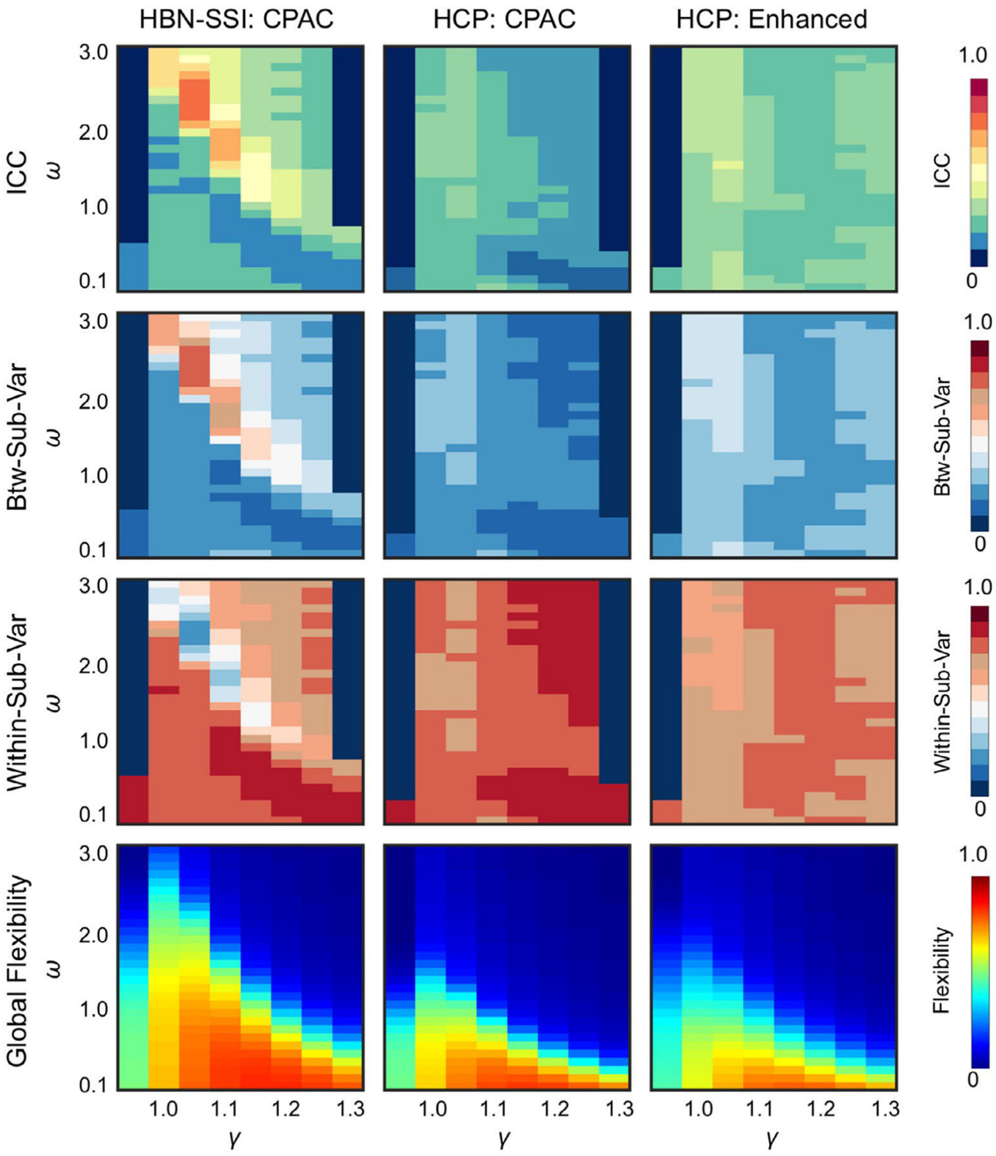

Fig. 5.

The $\gamma - \omega$ optimized for HBN-SSI cannot be generalized to HCP data. In HBN-SSI data, a range of parameters had good reliability (ICC ≥ 0.6). However, in HCP data, we were unable to find a range of parameters with good ICCs regardless of preprocessing pipelines (CPAC or HCP enhanced pipeline). As ICC was determined by both between-subject variance (Btw-Sub-Var) and within-subject variance (Within-Sub-Var), good ICCs in HBN-SSI overlapped with the portion of the landscape with high Btw-Sub-Var and low Within-Sub-Var. In HCP, the poor ICC was associated with low Btw-Sub-Var and high Within-Sub-Var. Furthermore, the two datasets also differed in global flexibility. The values dropped more quickly when ω increased for the HCP data than for the HBN-SSI data. Results were obtianed using 60 min of resting state data for test and retest.

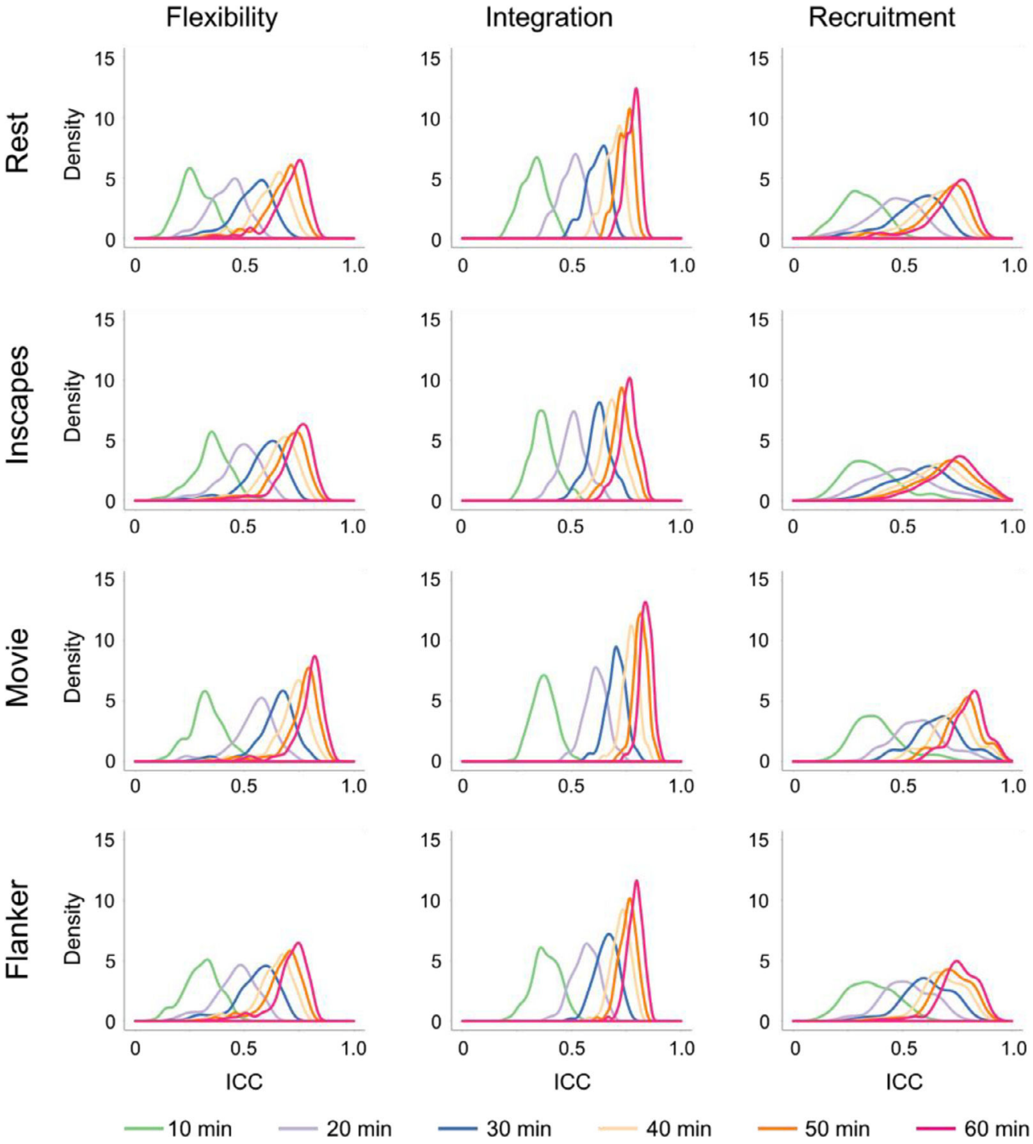

Fig. 6.

Test–retest reliability of dynamic network measures increases when the amount of data used for estimation increases. The density map of ICC values of 200 ROIs was plotted for three dynamic measures (flexibility, integration, and recruitment) and four tasks (rest, Inscapes, movie, and flanker) at six scan durations (10 min, 20 min, 30 min, 40 min, 50 min, and 60 min).

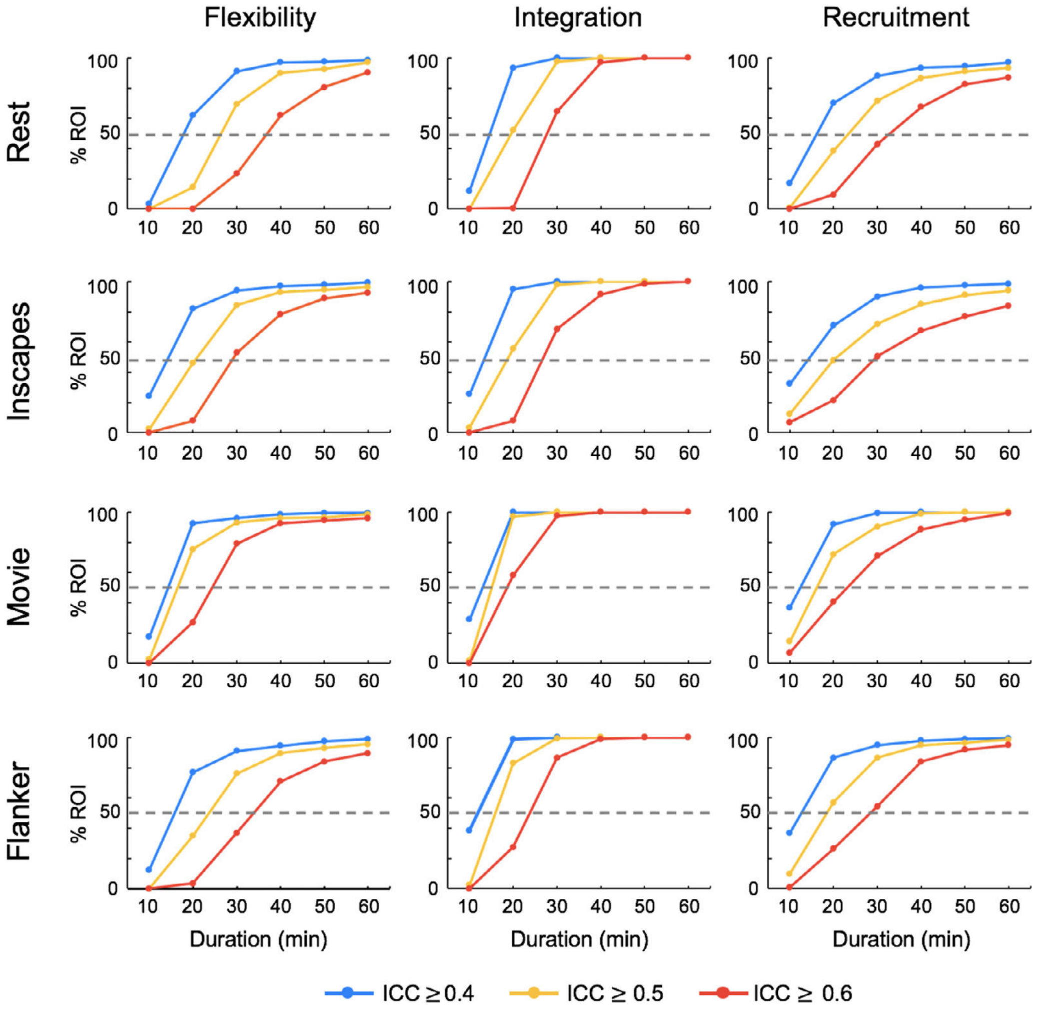

Fig. 7.

The minimal data requirements for sufficient reliability depending on the criteria, the measure, and the task. Percentage of ROIs with an ICC greater than 0.4 (blue line), 0.5 (orange line), and 0.6 (red line) were plotted for the three dynamic network measures (flexibility, integration, and recruitment) and the four tasks (rest, Inscapes, movie, flanker). The dashed gray line was drawn at 50%.

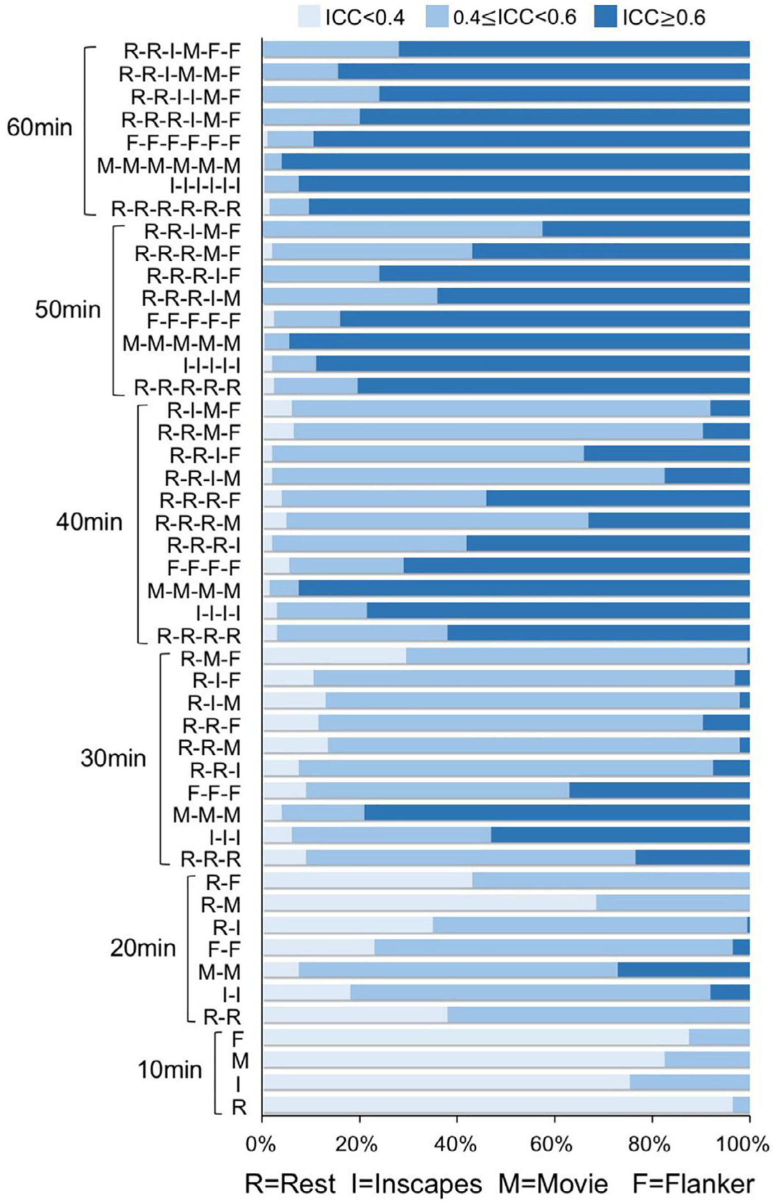

Fig. 8.

Combining data from different tasks improved reliability. Percent of ROIs showing poor (light blue: ICC < 0.4), fair (medium blue: 0.4 ≤ ICC < 0.6), or good (dark blue: ICC ≥ 0.6) reliability were plotted for six durations: 10 min, 20 min, 30 min, 40 min, 50 min, and 60 min. For each duration, the data can be a single condition or a combination of the four conditions: rest (R), Inscapes (I), movie (M), and flanker (F). Each letter (the abbreviation of each condition) represents 10 min of data.

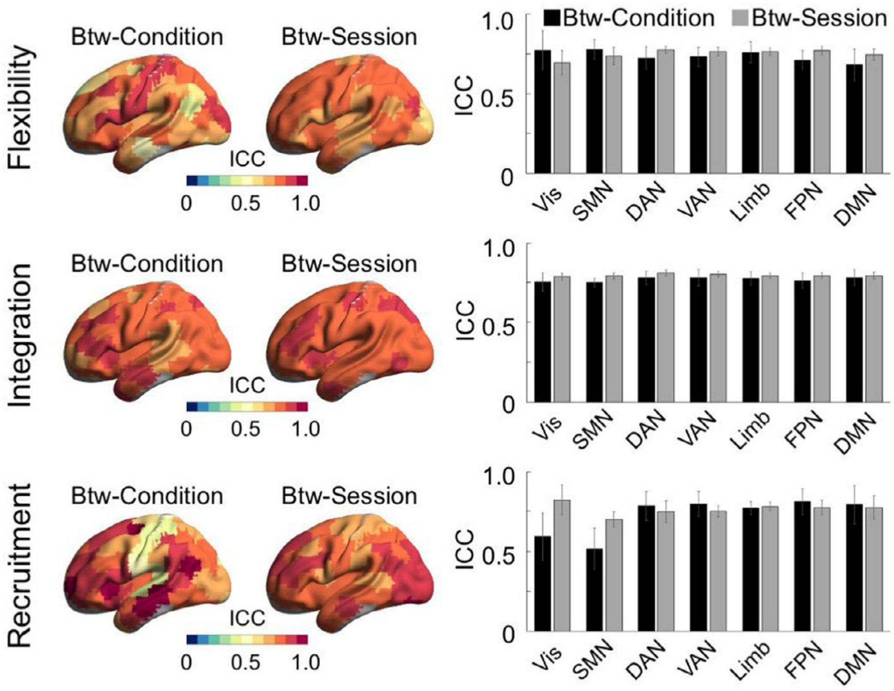

Fig. 9.

Both between-session and between-condition reliability evaluated in a hierarchical linear mixed model were good (ICC ≥ 0.6) to excellent (ICC ≥ 0.8) for 60 min of data. btw-condition: reliability among rest, Inscapes, movie, and flanker; btw-session: reliability between test and retest. ICCs were plotted on the surface map using BrainNet Viewer (Xia et al., 2013), as well as summarized per the seven networks defined by Yeo et al. (2011) in bar plots. Vis: visual network; SMN: somatomotor network; DAN: dorsal attention network; VAN: ventral attention network; Limb: limbic network; FPN: frontoparietal network: DMN: default mode network. The same network abbreviations were used for subsequent figures.

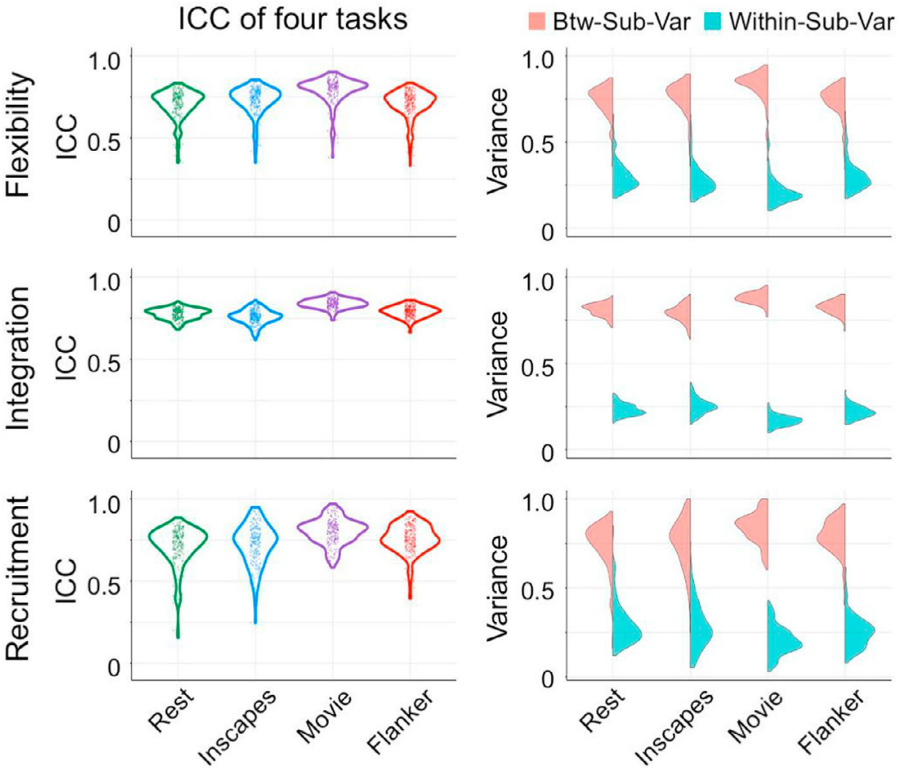

Fig. 10.

The movie condition was most reliable. Distribution of ICCs of 200 ROIs were plotted for four conditions (rest, Inscapes, movie, and flanker) in the left column. Density of between-subject variance (Btw-Sub-Var: salmon) and within-subject variance (Within-Sub-Var: light sea green) were plotted for each condition in the right column.

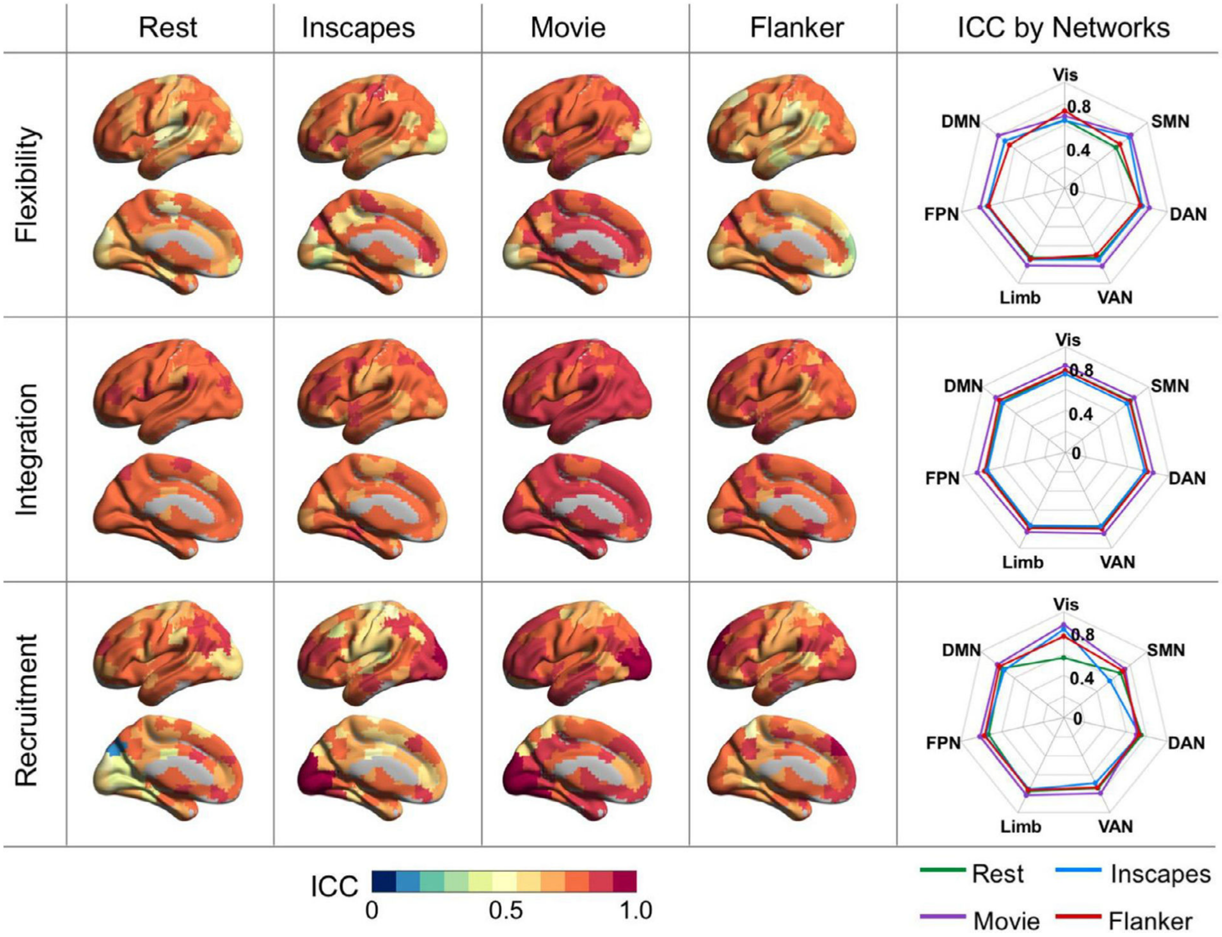

Fig. 11.

The impact of condition on the test-retest reliability of dynamic network measures. Spatial maps of ICCs for rest, Inscapes, movie, and flanker condition are shown on the brain surface for flexibility, integration, and recruitment. ICCs of 200 ROIs were averaged based on Yeo et al. (2011)'s seven networks for each of the four conditions and shown in the radar chart: Rest (green line), Inscapes (light blue line), Movie (purple line), and Flanker (red line).

Table 1

Summary of prior papers using flexibility, integration, or recruitment in the context of fMRI data.

Study	Task (Scan duration)	Edge estimation	γ	ω
Al-Sharoa et al. (2019)	Rest (8.8 min)	PCC	1	1
Bassett et al. (2011)	Motor learning (3.45 hrs)	PCC, wavelet coherence	1	1
Bassett et al. (2013b)	Motor learning (3.45 hrs)	wavelet coherence	1	1
Bassett et al. (2015)	Motor learning (3.45 hrs)	wavelet coherence	1	1
Betzel et al. (2017)	Rest (10 min/session, 91 sessions)	wavelet coherence	1	1
Braun et al. (2015)	Working memory (~5 min)	wavelet coherence	1	1
Braun et al. (2016)	Working memory (~5 min)	wavelet coherence	1	1
Chai et al. (2016)	Semantic relatedness judgment task (13.3 min), Story comprehension task (18~36 min)	PCC	1	0.5
Cocuzza et al. (2020)	Rest (14 min), Concrete permuted rule operations paradigm (~60 min)	PCC	1	1
Cole et al. (2014)	Dataset 1: Rest (10 min), Permuted rule operation cognitive paradigm (72 min) Dataset 2 (HCP): Rest (~60 min), 7 Tasks* (60 min total)	PCC	1	0–2
Cooper et al. (2019)	Persuasive messaging task (30.3 min)	wavelet coherence	NR	NR
Feng et al. (2019)	Rest (~8 min)	PCC	1	1
Fine et al. (2020)	Rest (40.8 min), N-back (46 min)	PCC	1	1, 0.5
Gerraty et al. (2018)	Reinforcement learning (25 min)	wavelet coherence	1.18	1
Gifford et al. (2020)	Rest (5 min)	PCC	1	1
Han et al. (2020)	Rest (8.5 min)	PCC	1	1
He et al. (2018)	Rest (5 min), Verbal generation task (5 min)	wavelet coherence	1	0.4
He et al. (2019)	Rest (~8 min)	PCC	1	1
Khambhati et al. (2018)	Rest (40 min)	multi-taper coherence	1	1
Lehmann et al. (2017)	Simulated rest (12 min)	PCC	1.25	2
			1.5	1
Li et al. (2019)	Rest (~6.7 min)	wavelet coherence	1	1
Lydon-Staley et al. (2019a)	Rest (6 min)	PCC	1	1
Lydon-Staley et al. (2019b)	Rest (6 min)	wavelet coherence	1	1
Mattar et al. (2015)	Rest (10 min), Permuted rule operation cognitive paradigm (72 min)	PCC	1	0.45
Pedersen et al. (2018)	Rest (HCP: ~60 min)	PCC	1	1

Study	Task (Scan duration)	Edge estimation	γ	ω
Schlesinger et al. (2017a)	Dataset 1: Recognition memory task (25.5 min) Dataset 2: Rest (6 min), attention task (20 min), memory task with lexical stimuli (22.5 min), face memory task (22.5 min)	wavelet coherence	1	1
Schlesinger et al. (2017b)	Word memory task (25.3 min)	wavelet coherence	1.2	0.05
			1.15	0.001
Shanmugan et al. (2020)	N-back (15.4 min)	wavelet coherence	1	1
Shao et al. (2019)	Rest (6.8 min)	least absolute shrinkage and selection operator (LASSO)	1	1
Shine et al. (2016)	Rest (10 min/session, 84 sessions)	multiplication of temporal derivatives (MTD)	1	1
Telesford et al. (2016)	Recognition memory (20 min), Strategic attention task (20 min)	wavelet coherence	1	1
Tian et al. (2019)	Rest (7 min)	PCC	1	0.25
Wei et al. (2017)	Rest (6.8 min)	conditional Granger causality	1	1
Wymbs et al. (2012)	Motor learning (3.45 hrs)	Inter-key interval (IKI)	0.9	0.03
Zheng et al. (2018)	Rest (8 min)	PCC	1	1

Note: PCC: Pearson’s correlation coefficient; γ: intra-layer coupling parameter; ω: inter-layer coupling parameter

[*] 7 tasks from HCP: emotional, gambling, language, motor, relational, social, and N-back tasks.

NR: not reported.

Table 2

Overview of the analysis performed in the paper.

Questions	Data	Analytical Approaches	Key Findings
Which modularity maximization method of the generalized Louvain algorithm is better suited for the analysis of multilayer networks in functional brain imaging data?	HBN-SSI (rest: 10 min/session, 12 sessions that were pseudorandomly split into a test and a retest dataset with 60-min each), $n = 10$ HCP test–retest dataset (rest: 15 min/run, 4 runs for test and 4 runs for retest), $n = 25$ Simulated data	Impact of modularity maximization methods on dynamic measures In HBN-SSI data, calculate three dynamic measures (flexibility, integration, and recruitment) using two modularity maximization methods (Modularity Maximization Method and Modularity Probability Method) across a range of ω [0.1 – 3.0] and γ [0.95–1.3]. Compare two algorithms by computing the between-algorithm reliability on each of the three measures. Replicate results in HCP and simulated data. Impact of modularity maximization methods on test–retest reliability of dynamic measures In HBN-SSI data, compare the ICC values on γ–ω plane obtained using two methods for each measure. Impact of modularity maximization methods on validity of dynamic measures In simulated data, compare the community changes obtained using the two methods and examine which one obtains results closer to the expected measures.	Modularity maximization methods have a large impact on the value of dynamic network measures and these effects can be replicated in an independent neuroimaging and non-neuroimaging dataset (Figs. 3 and S1). Modularity Probability Method results in higher test–retest reliability for dynamic network measures (Fig. S2). Modularity Probability Method recovers better the known underlying dynamics in simulated data (Figs. S3 and S4).
What are the optimal parameters for test–retest reliability?	HBN-SSI (rest, Inscapes, movie, flanker, each with 10 min/session, 12 sessions that were pseudorandomly split into a test and a retest dataset with 60-min each), $n = 10$ HCP test–retest dataset (rest: 15 min/run, 4 runs for test and 4 runs for retest), $n = 25$	Optimization of parameters for test–retest reliability Calculate ICCs for three measures and four task conditions across the γ–ω plane using Craddock 200 functional parcellation. Identify parameters resulting in peak ICC and with ICC>0.6. Compare our parameter selection optimized for reliability (γ=1.05 and ω=2.5) and previously recommended parameters (γ=1 and ω=1) Decompose ICC by assessing the within- and between-subject variability. Comparison of optimized parameters between functional parcellations Calculate ICCs across γ–ω plane for three measures during the movie condition using Schaefer 200 and Schaefer 600 parcellations. Assessing within- and between-subject variability calculated using each parcellation. Generalization of optimized parameters across datasets Calculate ICCs across γ–ω plane for flexibility during the rest condition using HCP data. Identify parameters resulting in peak ICC and with ICC>0.6. Compare ICCs across ω–γ plane between two datasets. Optimization of parameters for another reliability measure Calculate discriminability for three measures and four task conditions across the γ–ω plane. Identify parameters resulting in peak discriminability and with discriminability>0.9.	We identified an optimal range of parameters generalizable across tasks and measures and the parameters peak most across tasks and measures is γ=1.05 and ω=2.5 (Fig. 4). Previously recommended parameters (γ=1 and ω=1) resulted in high flexibility and low test–retest reliability (Fig. S5). The variations in test–retest reliability on the γ–ω plane is driven by the within and between-subject variability (Figs. S5 and S6). The selection of γ–ω is not sensitive to functional parcellations, but to the resolution of parcellation (Figs. S7 and S8). Optimized γ–ω based on HBN-SSI data cannot be generalized to HCP data (Fig. 5). The selection of γ–ω is sensitive to the criteria of optimization (e.g., reliability vs discriminability) and parameters optimized for discriminability are less consistent across tasks and measures (Fig. S9).
How much data is necessary for reliably estimating multilayer network dynamics?	HBN-SSI (rest, Inscapes, movie, flanker, each with 10 min/session, 12 sessions that were pseudorandomly split into a test and a retest dataset with 10-, 20-, 30-, 40-, 50-, and 60-min each), $n = 10$	Evaluation of ICC as a function of scan duration Calculate ICCs for three measures and four tasks with 10, 20, 30, 40, 50, and 60 min of data. Each duration was repeated 100 times on randomized samples to stabilize ICC values. Compute percent of ROIs with ICC>0.4, 0.5, 0.6. Visualize how the whole brain pattern of ICCs changes as a function of scan duration and summarize the change pattern based on Yeo et al. (2011)'s seven networks. The impact of combining task conditions on ICCs Compare ICCs obtained from 10 min of data from a single condition with	The minimal data requirement for dynamic network analysis for the movie condition is 20 min and 30 min for the other three conditions (Figs. 6 and 7). The regional and network-level variations in reliability as a function of scan duration are measure-dependent (Fig. S10). When data for one task is insufficient, we can combine different tasks to increase scan duration, and thus improve reliability (Fig. 8).

Questions	Data	Analytical Approaches	Key Findings
		longer data (20–60 min) created by adding more data either of the same condition or from different conditions.	
Which task condition is most reliable?	HBN-SSI (rest, Inscapes, movie, flanker, each with 10 min/session, 12 sessions that were pseudorandomly split into a test and a retest dataset with 60-min each), *n* = 10	Evaluation of ICC as a function of task condition For each measure, run hierarchical linear mixed models to assess between-condition (i.e., rest, Inscapes, movie, and flanker) and between-session (i.e., test, retest) reliability in the same model. For each measure, run simple linear mixed models for each task condition to assess between-session reliability. The significance of differences in reliability among task conditions were assessed using a nonparametric Friedman test. For each measure, assess the within- and between-subject variability of each task condition. Visualize how the whole brain pattern of ICCs changes as a function of task condition and summarize the change pattern based on Yeo et al. (2011)'s seven networks. The impact of frequency on ICC during the flanker task Compare ICCs obtained at low (0.01–0.1 Hz) and high (0.1–0.3 Hz) frequency during the flanker task.	Both between-session and between-condition reliability were high for 60 min of data, except that the between-condition reliability of recruitment within the visual and sensorimotor areas is medium (Fig. 9). The movie task is the most reliable (Fig. 10). Regional and network-level variations in reliability as a function of task conditions are measure-dependent (Fig. 11). The reliability of the flanker task is higher for the low frequency compared to the high frequency (Fig. S11).